The Direct Observation of Secondary Radical Chain Chemistry in the Heterogeneous Reaction of Chlorine Atoms with Submicron Squalane Droplets

Chen-Lin Liu,[1,2,#] Jared D. Smith,[1] Dung L. Che,[1,2] Musahid Ahmed,[1] Stephen R. Leone,[1,2,3] and Kevin R. Wilson[1,*]

[1] *Chemical Sciences Division, Lawrence Berkeley National Laboratory, Berkeley, CA 94720*

[2] *Department of Chemistry, University of California, Berkeley, CA 94720*

[3] *Department of Physics, University of California, Berkeley, CA 94720*

[#] *current address: National Synchrotron Radiation Research Center (NSRRC), Hsinchu 30076, Taiwan*

[*]Correspondence to: K. R. Wilson (krwilson@lbl.gov)

Abstract

The reaction of Cl atoms, in the presence of Cl_2 and O_2, with sub-micron squalane particles is used as a model system to explore how surface hydrogen abstraction reactions initiate chain reactions that rapidly transform the chemical composition of an organic particle. The heterogeneous reaction is measured in a photochemical flow tube reactor in which chlorine atoms are produced by the photolysis of Cl_2 at 365 nm. By monitoring the heterogeneous reaction, using a vacuum ultraviolet photoionization aerosol mass spectrometer, the effective reactive uptake coefficient and the distributions of both oxygenated and chlorinated reaction products are measured and found to depend sensitively upon O_2, Cl_2, and Cl concentrations in the flow reactor. In the absence of O_2, the effective reactive uptake coefficient monotonically increases with Cl_2 concentration to a value of ~3, clearly indicating the presence of secondary chain chemistry occurring in the condensed phase. The effective uptake coefficient decreases with increasing O_2 approaching a diffusion corrected value of 0.65 ± 0.07, when 20% of the total nitrogen flow rate in the reactor is replaced with O_2. Using a kinetic model it is found that the amount of secondary chemistry and the product distributions in the aerosol phase are controlled by the competitive reaction rates of O_2 and Cl_2 with alkyl radicals. The role that a heterogeneous pathway might play in the reaction of alkyl radicals with O_2 and Cl_2 is investigated within a reasonable range of reaction parameters. These results show, more generally, that for heterogeneous reactions involving secondary chain chemistry, time and radical concentration are not interchangeable kinetic quantities, but rather the observed reaction rate and product formation chemistry depends sensitively upon the concentrations and time evolution of radical initiators and those species that propagate or terminate free radical chain reactions.

I. Introduction

Chemical reactions occurring at interfaces govern a wide array of environmentally and technologically important processes ranging from soot formation and oxidation, aerosol aging, lipid peroxidation, corrosion, hydrocarbon cracking, and heterogeneous catalysis. In many of these systems free radicals play key chemical roles as initiators or propagators of surface reactions or as reactive intermediates. One of the first steps in hydrocarbon free radical chemistry is hydrogen abstraction that forms alkyl radicals whose subsequent reactions are key steps in radical chain reactions in combustion chemistry. In the atmosphere, the oxidation of alkyl radicals to alkylperoxy species form radical intermediates and stable reaction products, which are important steps in the photochemical production of smog and the formation and heterogeneous aging of organic aerosol.

While many aspects of homogeneous gas and liquid phase chemistry of free radicals are fairly well understood, there remains significant uncertainty about the heterogeneous reactivity of free radicals, such as OH and Cl, with organic surfaces composed of long chain hydrocarbons; these hydrocarbons are models for important chemical constituents of organic aerosols or biofuel droplets. A class of radical reactions in the gas phase that are particularly well characterized are hydrogen abstraction reactions of the general form shown in R1. The overall rate and mechanism of the reaction depends upon the molecular structure of RH as well as the abstracting species X.

$$RH + X\cdot \rightarrow R\cdot + HX \qquad \text{(R1)}$$

For example, the rate coefficient for hydrogen abstraction of ethane by Cl is 200 times faster than by OH. This difference decreases with normal alkane chain length. For decane the Cl reaction is only 40 times faster than that of OH. Different transition states and activation barriers are responsible for the large differences in hydrogen abstraction reaction rate coefficients. The large number of gas phase reactions measured for both Cl and OH has enabled the formulation of general rules for predicting rate coefficients based upon structure-reactivity

63 relationships.[1-2] However, it remains unclear whether rate coefficient predictions based upon
64 gas phase structure-reactivity relationships can be applied to heterogeneous reactions of Cl and
65 OH with large hydrocarbons at the surface of a liquid droplet. Although radical chain reactions
66 have been observed in many gas phase reactions, the high molecular density in an organic
67 aerosol or fuel droplet might be expected to enhance radical chain cycling mechanisms.

68 Although the main focus of this study is fundamental radical-particle reaction
69 mechanisms, there is some evidence in the literature that Cl atom chemistry could play a role in
70 certain regions of the troposphere. Although the global concentration of Cl is much lower than
71 OH, recent work has shown that Cl-initiated oxidation might be comparable to OH in coastal
72 and industrialized areas.[3] Chlorine atoms can be formed by the solar photolysis of reactive
73 chlorine species (e.g. $ClNO_2$, Cl_2, etc.), which in turn could be emitted from industrial sources
74 or produced via heterogeneous reactions.[4-5]

75 The rate of a heterogeneous reaction with a gas phase free radical (X) is expressed as a
76 reaction probability or uptake coefficient (γ_X), which is defined as the fraction of collisions
77 with a surface that results in a reaction. An uptake coefficient is directly obtained by measuring
78 the loss of a gas phase species (X) exposed to a hydrocarbon surface; in this case by definition
79 $\gamma_X \leq 1$. Rather than directly measuring the gas phase radicals that are often in very low
80 concentrations and hard to detect, an alternative approach is to monitor the reaction via the
81 condensed phase loss of the hydrocarbon (RH) to obtain an effective heterogeneous reaction
82 probability (γ_X^{RH}). Reactions on submicron organic aerosols are now commonly measured in
83 this way due in part to the wide availability of aerosol mass spectrometers that measure
84 changes in particle composition in real time.

85 If the loss of particle phase hydrocarbon (RH) is entirely due to reaction with the gas
86 phase radical (X) then the effective uptake coefficient is again by definition equal to γ_X and less
87 than or equal to 1 (i.e. $\gamma_X^{RH} = \gamma_X \leq 1$). Alternatively, if there are additional loss channels (e.g.
88 radical chain reactions) that consume RH in the condensed phase, then the effective uptake

coefficient (γ_X^{RH}) is no longer equivalent to γ_X, measured via the gas phase loss of the radical, but rather $\gamma_X^{RH} > \gamma_X$. Clear evidence for secondary chemistry is observed for specific cases where γ_X^{RH} exceeds unity. However, the magnitude of secondary chemistry cannot be ascertained merely by the absolute value of γ_X^{RH} but only in its relationship to γ_X.

Effective uptake coefficients larger than one have been observed by a number of groups measuring the radical-initiated oxidation of organic particles. Smith and coworkers measured effective uptake coefficients of 2.0 and 1.7 for the reaction of OH[6] and Cl[7] with dioctyl sebacate (DOS) particles in the presence of oxygen, respectively. McNeill et al. reported evidence for secondary chemistry in the OH oxidation of solid palmitic acid particles.[8] Although the uptake coefficient was found to be between 0.8 – 1, the presence of secondary chemistry was inferred using a kinetic model of their data. Another study by George et al.,[9] using DOS particles, reported an OH uptake coefficient larger than one (1.3 ± 0.4), but concluded, within experimental error, that there was no strong indication of secondary chemistry. In a smog chamber study of the OH oxidation of motor oil aerosol,[10] Weikamp and coworkers measured a wide range of effective uptake coefficients for a set of target compounds in the multi-component oil aerosol (e.g. hopanes and steranes). They measured uptake coefficients that ranged from 0.1 to 8. Lambe et al.[11] measured effective OH uptake coefficients for a variety of n-alkane, hopane and sterane marker molecules in motor oil and diesel aerosol. In this study, effective uptake coefficients between 1 and 40 were measured, with the higher volatility compounds exhibiting the largest reaction rates. The large effective coefficients were attributed to significant contributions of gas phase oxidation to the heterogeneous reaction rate.

For many of these systems the reaction pathway responsible for secondary chemistry currently remains unclear, but it has been proposed that radical intermediates, such as alkoxy radicals, could propagate chain reactions.[7] Once initiated by a hydrogen abstraction reaction at a surface, secondary chemistry can accelerate the overall rate of particle transformation, thus reducing chemical lifetime of an organic aerosol in the atmosphere.

The heterogeneous reaction of Cl atoms with submicron organic droplets composed of a branched alkane, squalane ($C_{30}H_{62}$), will be used to examine how (i) the heterogeneous reaction rate of Cl atoms compares with previous measurements of OH and (ii) how radical chain cycling mechanisms are manifested in measurements of effective uptake coefficients and reaction product distributions. The generalized reaction scheme considered here is,

$$RH + Cl_g \cdot \xrightarrow{\gamma_{Cl}} R \cdot + HCl \quad \text{(R2)}$$

$$R \cdot + Cl_{2_p} \xrightarrow{k_{3a}} RCl + Cl_p \cdot \quad \text{(R3a)}$$

$$R \cdot + Cl_{2_g} \xrightarrow{\gamma_{Cl_2}} RCl + Cl_p \cdot \quad \text{(R3b)}$$

$$RH + Cl_p \cdot \xrightarrow{k_4} R \cdot + HCl \quad \text{(R4)}$$

$$R \cdot + O_{2_p} \xrightarrow{k_{5a}} RO_2 \cdot \quad \text{(R5a)}$$

$$R \cdot + O_{2_g} \xrightarrow{\gamma_{O_2}} RO_2 \cdot \quad \text{(R5b)}$$

$$RO_2 \cdot + RO_2 \cdot \xrightarrow{k_6} Alcohol + Ketone + O_2 \quad \text{(R6)}$$

$$RO_2 \cdot + RH \xrightarrow{k_7} ROOH + R \cdot \quad \text{(R7)}$$

where the subscripts p and g denote condensed (particle) and gas phase species, respectively. In this respect a number of the reaction pathways (e.g. R3a vs. R3b) can occur either at the surface of the particle or within the liquid as shown schematically in Fig. 1. For example, the alkyl radical, $R \cdot$, initially formed by gas phase hydrogen abstraction reaction by Cl · (R2), could react in the liquid phase (i.e. homogeneously) with Cl_2/O_2 dissolved in the particle as shown by R3a and R5a and schematically in Fig. 1. For this case the rates of R3a and R5a are proportional to the total concentration of Cl_2 and O_2 within the particle, which in turn is determined by the Henry's Law constant for these species in squalane. Alternatively, the $R \cdot +$ Cl_2 (and O_2) reaction(s) could occur heterogeneously by the gas phase collision of Cl_2 (O_2) with an alkyl radical at the particle surface as illustrated by R3b and R5b and schematically in Fig. 1.

For this case, the reaction rates depend upon the reactive collision frequency of gas phase Cl_2/O_2 with the particle surface. The relative importance of these parallel reaction pathways (termed homogeneous and heterogeneous) will be considered later using the kinetic model described in Sec. III.C.

R2 is the heterogeneous reaction of gas phase chlorine atoms ($Cl_g\cdot$) that initiates the chemistry in the organic particle (Fig. 1). Based upon gas phase structure-reactivity relationships, the predicted rate coefficient for the Cl reaction will be ~32 times larger for squalane than OH.[1] Although there remains some controversy about the exact magnitude of the OH reactive uptake coefficient onto organic surfaces, since values between 0.1 and 8 have been reported, there is definitely not a 32 times enhancement of the reaction probability of Cl over OH. This then suggests that the reactivity of organic surfaces towards gas phase radicals is not merely determined by gas phase structure-reactivity relationships, but rather by more subtle features at the organic interface.

For the mechanism (R2-R7) shown schematically in Fig. 1, chain propagation occurs via R3 and R4, since Cl_2, the radical precursor, can react with R· regenerating a Cl atom in the particle phase (denoted $Cl_p\cdot$), which participates in further hydrogen abstraction reactions (R4). In the presence of O_2, R5 competes with R3 by forming an alkyl peroxy radical instead of a chlorinated alkane and $Cl_p\cdot$. The alkyl peroxy self-reaction (R6) is the dominant loss channel for this species in a particle exposed to high radical concentrations ($>10^9$ molec cm^{-3}), detailed in our previous study.[12] In the condensed phase, R6 is generally thought to produce stable reaction products, such as alcohols and ketones, which terminate the radical chain reaction. For small molecules in the gas phase, the alkyl peroxy self-reaction can also form two alkoxy radicals.[13-14] These radical intermediates if formed in the particle could play a role in chain propagation chemistry. Since there remains little direct evidence that alkoxy radicals are formed in the condensed phase[15-18] this reaction is not explicitly considered here. The condensed phase rate constant for hydrogen abstraction by $RO_2\cdot$ (i.e. another channel of

164 secondary reaction) is small (R7).[19] Therefore the amount of secondary chemistry occurring in
165 the organic particle is controlled mainly by the relative reaction rates of R3 and R5, which can
166 be experimentally investigated by changing the amount of oxygen available in the reaction.

167 There are a few experimental measurements of the reaction probability of gas-phase Cl
168 radicals with condensed-phase organic compounds. Moise and Rudich measured the first order
169 loss of Cl above alkane and alkene monolayers and determined that the reactive uptake
170 coefficient was near the collision limit ($0.1 < \gamma_{Cl} < 1$).[20] Hearn et al.[7] observed the Cl effective
171 uptake coefficient on organic particles to be 1.7 and 0.9-1.7, with and without O_2 present,
172 respectively. Although Hearn and coworkers acknowledge the importance of R3 for chain
173 cycling reactions in the absence of O_2, they do not report the presence of chlorinated reaction
174 products or explicitly show how chlorine chain chemistry influences their reported effective
175 uptake coefficients or the evolution of reaction products as a function of O_2 concentration.

176 The heterogeneous reaction of Cl atoms with submicron squalane droplets is measured in a
177 photochemical aerosol flow reactor using a vacuum ultraviolet photoionization time-of-flight
178 aerosol mass spectrometer (VUV-AMS). Aerosol mass spectrometry is used to measure
179 heterogeneous reaction rates and product distributions needed to formulate a detailed reaction
180 mechanism that includes secondary chemistry. In Section III.A, the competition between the
181 R3 and R5 reaction channels will be explored by measuring effective uptake coefficients as a
182 function of $[O_2]$ in the flow reactor. In Section III.B, measurements of how $[Cl_2]$ and [Cl]
183 influence the heterogeneous reaction are presented. In Section III.C, a kinetic model is
184 formulated to explain the overall reaction mechanism and product distribution. The kinetic
185 model will be used to explore where key propagation and termination reactions (e.g R3a and
186 R5a vs. R3b and R5b) occur: either as a homogeneous reactions in the interior of the particle or
187 via heterogeneous reactions at the aerosol surface. Finally, the chemical evolution of the
188 chlorinated reaction products is presented (Section III.D) and compared with detailed
189 predictions using the kinetic model.

II. Experimental

Since a detailed description of the experiment setup has been given in a previous study,[12] only a brief update is indicated here. An atmospheric pressure flow tube reactor, shown in Fig. 2, is used to investigate the heterogeneous reaction of squalane particles. Aerosol is formed by homogeneous nucleation of the organic vapor in a N_2 stream flowing through an ~45 cm long Pyrex tube containing liquid squalane. The Pyrex tube is heated in a tube furnace to ~130 °C producing a log-normal particle size distribution with a mean surface-weighted diameter of ~180 nm and a geometric standard deviation of ~1.3. Cl_2, O_2, and the trace reference compounds (acetone or 2-butanone) are mixed with the aerosol stream in a balance of N_2 prior to entering the flow tube reactor. The concentrations of Cl_2 and O_2 are reported here as flow ratios, i.e. the volume concentration. For example, 20% O_2 is obtained when 0.22 L/min of the total 1.1 L/min flow is O_2. For the experiments without O_2, a scrubber (0.75 L Supelpure-O trap) is placed in the nitrogen lines to reduce residual oxygen levels to less than 0.05%. The mixed gases and particles are then introduced into a 130 cm long, 2.5 cm inner diameter type 219 quartz reaction cell. Cl atoms are generated along the length of the reaction cell using one to four continuous output 130 cm long black light (λ = 365 nm) lamps (UVP, LLC.), which surround the flow tube reactor. The total flow rate through the flow tube is 1.1 L/min, which corresponds to a reaction time of ~33.5 s. The Cl concentration is controlled by adjusting the molecular chlorine (Cl_2) concentration (5-40 ppm) and/or the photon flux in the flow tube reactor.

A fraction of the flow exiting the reactor is sent to a gas chromatograph (GC) equipped with a flame ionization detector (SRI Instruments) to monitor the decay of the gas phase reference compounds. The Cl exposure in the flow tube is determined via the removal of the gas phase reference compounds by reaction with Cl. The reference compounds used in these experiments are acetone (C_3H_6O) and 2-butanone (C_4H_8O), which react with Cl radicals with rate constants of 2.09 x 10^{-12} $cm^3 \cdot molec^{-1} \cdot s^{-1}$ and 3.66 x 10^{-11} $cm^3 \cdot molec^{-1} \cdot s^{-1}$, respectively.[9, 21]

The concentration of acetone or 2-butanone entering the reactor is 130 ppb – 230 ppb. The flow sampled by the GC is filtered to remove particles and passed through a small column packed with potassium carbonate to remove Cl_2. To detect ppb levels of the reference compounds, the flow is pre-concentrated for 3 minutes in a Tenax-GR absorbent trap before GC analysis.

The chemical composition of the aerosol is monitored with a custom-built vacuum ultraviolet aerosol mass spectrometer (VUV-AMS). This instrument measures aerosol composition by thermally vaporizing the aerosol (100 °C) followed by VUV photoionization (10 eV) as described by Gloaguen et al.[22] Tunable VUV radiation is produced by the Chemical Dynamics Beamline at the Advanced Light Source. The particle size distribution and number concentration are measured simultaneously using a scanning mobility particle sizer (SMPS, TSI model 3936).

The rate constant (k_{sq}) for the Cl reaction with squalane aerosol is determined using a standard relative rate approach using the formalism described by Smith et al.[12] The normalized decay of squalane in the particle phase is,

$$\frac{[Sq]}{[Sq]_0} = \exp(-k_{Sq}\langle Cl\rangle_t \cdot t) \quad (8)$$

where $[Sq]$ and $[Sq]_0$ are the final and initial concentrations of squalane, respectively. $\langle Cl\rangle_t$ is the time (t) average concentration of Cl atoms in the flow reactor. The chlorine atom exposure ($\langle Cl\rangle_t \cdot t$) is obtained from the concentration of the reference compounds (e.g. [Acetone]) measured before and after the reaction and is expressed as,

$$\langle \mathrm{Cl}\rangle_\mathrm{t} \cdot \mathrm{t} = \int_0^\mathrm{t}[\mathrm{Cl}]\mathrm{dt} = \frac{\ln([Acetone]/[Acetone]_0)}{-k_{Acetone}} \quad (9)$$

Assuming that k_{Sq} is independent of [Cl], $[Sq]/[Sq]_0$ is plotted versus $\langle Cl\rangle_t \cdot t$ and fit to an exponential function to determine k_{Sq}. For many of the kinetic measurements described below the Cl exposure is changed by keeping the flow rate (i.e. reaction time) constant and varying the average Cl concentration in the flow tube by changing the black light flux and therefore the

240 photolysis rate of Cl_2.

241 For other experiments conducted in the absence of O_2, the reaction rate is observed to
242 depend upon absolute Cl atom concentrations in the flow tube reactor, as will be discussed in
243 Sec. III.B. To isolate this dependence, the chlorine atom exposure is changed by modifying the
244 reaction time rather than the chlorine atom concentration as described above. This is done by
245 fixing the flow rate and moving an opaque curtain along the flow tube to change the length of
246 the illuminated reaction zone and therefore the reaction time. If there is a uniform
247 concentration of chlorine atoms along the length of the flow tube, then the resulting exposure is
248 linearly proportional to the residence time of the aerosol in the portion of the flow reactor
249 exposed to the black lights. This assumes that the Cl_2 photolysis rate is the same at all points
250 along the length of the flow reactor. Shown in Fig. 3 are measurements of Cl exposure as a
251 function of illuminated reactor length. For regions of the flow tube reactor near the end of the
252 flow tube where the lamp terminals are located, it is found that the chlorine exposure is not a
253 linear function of illumination length. However, more uniform illumination, and therefore
254 more uniform [Cl], is observed when the illumination length is greater than 33 cm and the
255 chlorine exposure becomes a linear function of illumination length (i.e. reaction time). For the
256 experiments reported here all measurements are recorded over a series of lengths where the
257 chlorine exposure is found to be a linear function of illumination length.

258 Heterogeneous kinetics is quantified by monitoring the decay of squalane in the organic
259 particle as a function of chlorine exposure. An exponential fit to such decay data yields, k_{Sq}, the
260 second order rate constant for the reaction. An effective reactive uptake coefficient (γ_{Cl}^{Sq}) can
261 be defined as the fraction of chlorine atom collisions with squalane in the particle phase that
262 yield a reaction. Using a formalism, originally developed by Smith et al.[12] for the OH +
263 squalane reaction, the reaction probability can be written as,

$$\gamma_{Cl}^{Sq} = \frac{4 \cdot k_{Sq} \cdot D_{surf} \cdot \rho_0 \cdot N_A}{\bar{c} \cdot 6 \cdot M_{Sq}}. \quad (10)$$

where D_{surf} is the mean surface-weighted particle diameter, ρ_0 is the initial squalane density (0.8 g·cm^{-3}), N_A is Avogadro's number, $\bar{c}$ is the mean speed of gas phase Cl, and M_{Sq} is the molar mass of squalane (422 g/mole).

For a fast surface reaction on a particle that is well-mixed on the timescale of the reaction, it can be assumed that the squalane decay rate (d[Sq]/dt) is directly proportional to the concentration of squalane in the particle as shown by Smith et al.[12] for the squalane + OH reaction. Since both the average chlorine atom concentration ($\langle Cl \rangle_t$ in Eq. (9)) and reaction time are very similar to those used in the OH study, the use of Eq. (10) is expected to be a valid method for analyzing the results presented here.

This particular formulation of the uptake coefficient is narrow, assumes a well mixed particle, and isolates the reaction probability of a single species from the reactivity of the entire particle itself. As the reaction progresses the particle composition evolves from pure squalane to chlorinated and/or oxygenated reaction products. In this case, a direct comparison of the squalane reaction probability (γ_{Cl}^{Sq}) with that of subsequent reaction products (e.g. $\gamma_{Cl}^{SqCl_n}$) is done in a systematic way to draw more general conclusions about how the effective uptake changes as the reaction proceeds and the aerosol is chemically transformed.

III. Results and discussion

The 10 eV photoionization mass spectra of squalane before and after reaction are shown in Figures 4(a) and (b), respectively. Before the reaction, the mass spectrum consists of two main peaks: the squalane molecular ion (*m/z* = 422) and a fragment peak located at *m/z* = 238. These two peaks are used to monitor the heterogeneous reaction. After reaction these peaks decrease and the formation of new reaction products are clearly observed. Once formed by the initial hydrogen abstraction by Cl·, the resulting R· radical can then in turn react with either O_2 or Cl_2

or both as illustrated by R3 and R5, forming a mixture of both the oxygenated and chlorinated reaction products. This is shown in Fig. 4(c), where there are two distinct groups of reaction products. The products containing oxygen functional groups are separated by 14 mass units as was observed previously[12, 23] for the OH + squalane reaction. In contrast, chlorinated reaction products are separated by an average of 34 amu, due to the addition of Cl and the loss of H, which is discussed below. In addition to the reaction products containing purely oxygen or chlorine functional groups, there is clear evidence for a significant number of reaction products that contain a mixture of both of these species as will be discussed below. The exact populations of the various products are a sensitive function of reaction conditions and are found to depend mainly upon the relative concentration of Cl_2 and O_2 in the flow reactor.

Shown in Fig. 5 are 10 eV photoionization mass spectra of the particle phase reaction products as a function of O_2 concentration. For each mass spectrum, the Cl_2 concentration is fixed at 32.7 ppm. At ~0% O_2, the mass spectrum (Fig. 5(a)) is dominated by chlorinated products denoted as $SqCl_n'$ as well as a peak located at two mass units smaller than squalane. The "prime" is used here to identify the ions ($SqCl_n'$ and Sq-2′) observed in the mass spectrum. These ions are formed via dissociative photoionization through the elimination of HCl. For example, the peak at m/z = 454 denoted SqCl′ does not correspond directly to the neutral SqCl molecular product (molecular weight = 456) but rather corresponds to the $SqCl_2$ molecule which undergoes dissociative photoionization by losing HCl.

As [O_2] is increased, new peaks appear corresponding to the formation of oxygenated reaction products (denoted SqO_n). At [O_2] ~ 0.3% the intensities of SqO_n and $SqCl_n'$ products are nearly equal, and by [O_2] = 5% the $SqCl_n'$ products are no longer visible and the mass spectrum is dominated by the oxygenated species. This sequence of mass spectra shows that, as expected, there are competing pathways for the formation of chlorinated and oxygenated reaction products that are sensitive to the amount of O_2 in the flow reactor. This competition naturally arises since both Cl_2 and O_2 can react with the alkyl radical that is formed by the

initial hydrogen abstraction reaction.

To investigate a highly coupled reaction mechanism that forms both chlorinated and oxygenated reaction products (shown in Fig. 5), we first present effective uptake coefficient measurements as a function of [O_2] (Sec. III.A). The reaction kinetics and product distributions at 20% [O_2] are then directly compared with the OH + squalane reaction.[12] The role that [Cl_2] and [Cl] play in the heterogeneous reaction will then be considered in Section III.B. In Section III.C a kinetic model with a global reaction mechanism is presented that explores how the reaction probability and the product formation kinetics depend upon Cl_2, O_2 and Cl. The kinetic model is parameterized to explore whether the overall mechanism (e.g. $R\cdot + Cl_2/O_2$) occurs as either a homogeneous reaction within the bulk particle or a heterogeneous reaction at the surface. The more complex chemical evolution of the purely chlorinated products when O_2 is absent is presented in Sec. III.D.

A. Effective Uptake Coefficient vs. [O_2]

The normalized decay of squalane ([Sq]/[Sq]$_0$), as a function of Cl exposure in the presence of large and small O_2 concentrations, is shown in Fig. 6. The decay constant, k_{Sq} is obtained from an exponential fit to the decay traces shown in Fig. 6. The effective uptake coefficient is then computed using Eq. (10). Effective uptake coefficients are plotted as a function of [O_2] for two different Cl_2 concentrations (14.5 and 32.7 ppm) in Fig. 7. For each Cl_2 concentration the effective uptake coefficient is a strong function of [O_2] and increases rapidly when the oxygen concentration in the flow tube is reduced to less than 1%. For these reaction conditions, the products, shown in Figures 5(a) and 5(b), are dominated by chlorinated functional groups. The absolute magnitude of the effective uptake coefficient, at low [O_2], depends upon the Cl_2 concentration, reaching a value larger than 3 for the 32.7 ppm case. Uptake coefficients larger than one provide clear evidence of chain cycling chemistry in the particle phase.

For both chlorine concentrations (14.5 and 32.7 ppm) the effective uptake coefficient

decreases rapidly with increasing [O_2] and then plateaus at ~0.57 for [O_2] > 2%. In this region (2% < [O_2] < 20%), the effective uptake coefficient no longer depends upon the amount of Cl_2 in the flow reactor and the reaction products in the particle are composed exclusively of oxygenated species as shown in Fig. 5(d). In the conditions of high [O_2] (e.g. [O_2] > 5%), R5 becomes the dominant reaction pathway for R·, effectively shutting down R3, the Cl chain reaction that produces chlorinated reaction products. At 20% O_2, only a small fraction (< 4%) of the measured effective uptake coefficient, $\gamma_{Cl}^{Sq} = 0.57$, is due to chlorine secondary chemical reactions, as will be described in Section III.C. γ_{Cl}^{Sq} is corrected for gas phase diffusion using the Fuchs and Sutugin formulation.[24-25] Here the gas phase diffusion coefficient of Cl·$_g$ in Ar ($D_{Cl-Ar} = 0.19$ cm^2 s^{-1}) is used for the correction instead of Cl·$_g$ in nitrogen, which to our knowledge has not been measured.[26-27] Recently, very good agreement between measured and calculated diffusion coefficients for OH radicals was published,[28] and by using the same formula we obtained the same value of diffusion coefficient (0.19 cm^2 s^{-1}) for Cl·$_g$ in N_2. The effective uptake coefficient at 20% O_2, corrected for the gas phase diffusion, is γ_{Cl}^{Sq} =0.65±0.07.

In previous work, the uptake coefficient for the OH + squalane reaction[12] was measured to be $\gamma_{OH}^{Sq} = 0.30 \pm 0.07$ at an average [OH] = 1 x 10^{10} molec·cm^{-3}, which is comparable to the average chlorine atom concentrations (1.5 x 10^{10} molec·cm^{-3}) used here. At lower OH concentrations ([OH] = 1-7 x 10^8 molec cm^{-3}) a larger effective uptake coefficient (γ = 0.51 ± 0.10) was measured by us, suggesting an additional loss channel for squalane in the particle phase that appears to compete with OH at low oxidant concentrations and longer reaction times.[23] The molecular origin of the chain chemistry in the OH + squalane reaction is still under investigation by us.

From simple gas phase structure reactivity relationships, it is expected that Cl atoms, in the absence of secondary chain chemistry that is effectively suppressed at 20% O_2, would react ~32 times faster with squalane compared to OH.[1-2] However, we observe that the Cl

heterogeneous reactive uptake is only ~2.2 times larger than the reactive uptake of OH, suggesting that more subtle features of the organic interface, such as the formation of a long-lived surface complex, might be controlling heterogeneous reactivity. In fact it has been noted by various authors that surface reactions by small radicals or atoms can be enhanced by several orders of magnitude over analogous bimolecular reactions in the gas phase. Moise and Rudich[20] measured the largest surface enhancement factors for gas phase reactions that are slow ($k < 10^{-15}$ $cm^3 \cdot molec^{-1} \cdot s^{-1}$) due to high activation energies, in contrast with fast reactions ($k \sim 10^{-12}$ $cm^3 \cdot molec^{-1} \cdot s^{-1}$), which exhibit minimal surface enhancement. For example, the surface reactions of Br and $O(^3P)$ atoms with an aliphatic monolayer were found to be enhanced by 10^4 to 10^3, respectively, over the analogous reactions in the gas phase. The mechanism for this surface enhancement is currently unclear, but may originate, in part, from multiple scattering, or trapping of reactant species at the interface, thus increasing the overall chance of a reactive encounter.[29-31] Within this context, it seems likely that the OH reaction is more enhanced at the squalane interface than Cl.

The kinetic evolution of squalane and its first three generations of oxidation products (SqO, SqO_2 and SqO_3) as a function of chlorine exposure, at 20% O_2, are shown in Fig. 8. The first three oxidation products are denoted generally as SqO_n, where n corresponds to the number of oxygenated functional groups added to the squalane molecule. As discussed in our previous publication on OH, these species (denoted generally as SqO_n) correspond to the formation of closed shell molecules containing alcohol and ketone functional groups as shown in R6.[12, 23] Here n designates the number of these oxygenated functional groups added to the squalane molecule. However, quantifying the absolute abundance of these individual molecular species (ketones vs. alcohols) in the particle requires VUV photoionization cross sections and fragmentation patterns, which are currently not known.

Nevertheless in our previous studies,[12, 23] it was found that the reaction products evolve sequentially via a statistical oxidation mechanism in which 1 oxygenated functional group is

added per reactive collision. For the Cl reaction at 20% O_2, the reaction products are entirely composed of molecules with oxygenated functional groups (SqO_n) similar to those observed in the OH + squalane reaction. Under these reaction conditions it is expected that these stable oxidation products will evolve via the same sequential oxidation mechanism, which can be written overall as,

$$SqO_n + Cl + \frac{1}{2}O_2 \xrightarrow{k_{Sq}} SqO_{n+1} + HCl \quad (11)$$

where k_{Sq} is the second order rate constant and n denotes the product generation. For squalane itself, n = 0. Previously, it was found that this simple reaction sequence, in which squalane and its oxidation products are assumed to react with the same rate coefficient (k_{Sq}), could account for the overall chemical transformation of squalane aerosol when exposed to OH.[12, 23] For the Cl reaction, the integrated equation corresponding to Eq. (11) is,

$$\frac{[SqO_n]}{[Sq]_0} = B_n \frac{(k_{Sq}\cdot\langle Cl\rangle_t\cdot t)^n}{n!}\exp(-k_{Sq}\cdot\langle Cl\rangle_t\cdot t) \quad (12)$$

where B_n is an adjustable parameter to account for differences in isotope abundance, VUV photoionization efficiency, and fragmentation patterns of the oxidation products and squalane. To fit the experimental data, k_{Sq} in Eq. (12) is first fixed to the value obtained from an exponential fit to the squalane decay curve shown in Fig. 8(a). The kinetic evolution of the oxidation products (SqO, SqO_2, and SqO_3) are then modeled, using Eq. (12), by adjusting a single parameter, B_n. Model fits to the experimental data are shown as solid lines in Fig. 8. As with the OH + squalane reaction, the sequential oxidation model captures, within experimental error, the overall kinetic evolution of the first three generations of products using a single rate constant. This then indicates that for the Cl + squalane reaction, at 20% O_2, $\gamma_{Cl}^{Sq} = 0.65 \pm 0.07 \approx \gamma_{Cl}^{SqO} \approx \gamma_{Cl}^{SqO_2} \approx \gamma_{Cl}^{SqO_3}$. Although the Cl effective uptake coefficient is ~2.2 times larger than that for OH, the kinetic evolution of the particle is consistent with that reported by us for the OH + squalane reaction.[12, 23]

Shown in Fig. 8 are arrows indicating the chorine exposures that correspond to 1, 2, and 3

417 squalane lifetimes ($\tau = 1/k_{Sq}$). At one lifetime $[Sq]/[Sq]_0 = 1/e$ and the first oxidation product
418 (SqO) has reached its maximum value. This is also the point in the reaction when the number of
419 reactive collisions is equivalent to the total number of molecules in the particle. The SqO_2
420 product peaks at 2 lifetimes ($[Sq]/[Sq]_0 = 1/e^2$), etc. Under these conditions, there is a simple
421 relationship between the squalane lifetime and the point in the reaction where each oxidation
422 product reaches its maximum value. This is a natural consequence of sequential oxidation in
423 which each component in the particle (Sq, SqO SqO_2, SqO_3) can be described using the same
424 rate coefficient as shown in Eq. (12). As will be shown below, a more complex relationship
425 between squalane lifetime and the kinetic evolution of the products is observed at low $[O_2]$
426 where the chlorinated reaction products are formed and secondary radical chain chemistry
427 controls the rate of the reaction.

428 **B. Effective uptake coefficient vs. $[Cl_2]$ and [Cl]**

429 As shown in Fig. 7, the uptake coefficient increases steeply when $[O_2]$ is reduced to <1%.
430 In the absence of oxygen, the squalane radical can react with Cl_2 to generate a chlorinated
431 product and a Cl atom, which is assumed to remain solvated in the particle ($Cl_p\cdot$) to participate
432 in further secondary reactions. If alternatively the $Cl_p\cdot$ escapes from the particle back into the
433 gas phase it would be detected as a primary $Cl_g\cdot$ by the gas phase tracer compound (i.e. acetone).
434 Under these conditions no secondary chain reactions (i.e. effective uptake coefficient larger
435 than one) would be observed. However, in the particle this radical intermediate ($Cl_p\cdot$) can react
436 with Sq, $SqCl_n$ and SqO_n (when O_2 is present), thus accelerating the rate at which the particle is
437 chemically transformed. From R3a and R3b, it is expected that this rate would be proportional
438 to the gas phase Cl_2 concentration in the flow reactor since the condensed phase chlorine (Cl_{2_p})
439 concentration or reactive collision frequency is proportional to the gas phase Cl_2 concentration.
440 To examine this dependence, effective uptake coefficients are measured as a function of Cl
441 exposure. For this set of measurements the reaction time and Cl_2 concentration are fixed and
442 the chlorine atom concentration is changed by varying the photon flux (i.e. the voltage supplied

443 to the black lights) in the reaction volume.

444 A typical decay trace of squalane, at low [O_2], is shown in Fig. 6. Under these reaction
445 conditions it was found that the decay of squalane is slightly non-exponential (i.e.
446 biexponential). This is because, in addition to [Cl_2], the secondary chain reaction also depends
447 upon the absolute Cl atom concentration in the flow tube, as will be detailed below. For
448 simplicity, single exponential fits are used to extract the uptake coefficients shown in Fig. 9.
449 Approximating the decay traces as single exponential functions leads to an overall error in the
450 computed uptake coefficients of 6 - 9%, which is not expected to change the overall results
451 presented here. Shown in Figure 9 are measurements of the effective uptake coefficients as a
452 function of [Cl_2]. At low Cl_2 concentrations (8 ppm) γ_{Cl}^{Sq} is less than 1 and monotonically
453 increases to a value of ~3 at [Cl_2] = 32.7 ppm.

454 In order to better isolate how the effective uptake coefficient depends explicitly upon
455 absolute [Cl], it is necessary to measure the reaction at a fixed [Cl_2] and [Cl] in the flow reactor.
456 This is done by changing the reaction time, and therefore Cl exposure, using an opaque curtain
457 as described above in Section II. A series of [Cl] dependent effective uptake coefficients, at
458 [Cl_2] = 14.5 ppm, are shown in Fig. 10. The effective uptake coefficient is observed to be
459 inversely proportional to the absolute Cl atom concentration in the flow reactor. At [Cl] =
460 2.67×10^9 molec/cm^3, γ_{Cl}^{Sq} is determined to be 2.5 and decreases to 1.4 when the concentration
461 is increased to 2.2×10^{10} molec/cm^3.

462 A radical termination step is proposed to explain this inverse dependence of γ_{Cl}^{Sq} on Cl
463 atom concentration, shown in Fig. 10. For example, there is some probability that two Cl_p·
464 atoms in the particle phase collide and recombine via the following reaction,

465 $$Cl_p\cdot + Cl_p\cdot + \mathrm{M} \xrightarrow{k_{13}} Cl_{2_p} + \mathrm{M}. \qquad \text{(R13a)}$$

466 where $Cl_p\cdot$, Cl_{2_p}, and M are the Cl atom, Cl_2, and third body collision partner (i.e. squalane
467 and its products), respectively. Without R13a, the effective uptake coefficient, under oxygen

free conditions, would become exceedingly large (e.g. $\gamma_{Cl}^{Sq} > 7$). Alternatively, with R13a, the chain reaction is arrested since there is a natural competition between the production of the $Cl_p\cdot$ atoms, which propagate the chain reaction via R3 and the terminating $Cl_p\cdot$ atom recombination step (R13a).

By using the steady state approximation to calculate the concentrations of $Cl_p\cdot$ and $R\cdot$ relative to $Cl_g\cdot$ when O_2 is absent, the recombination rate of R13a (i.e. the termination reaction) is found to be proportional to $[Cl_p\cdot]^2 \propto [Cl_g\cdot]$. The propagation reaction rate is directly proportional to the Cl concentration in particle, i.e. $[Cl_p\cdot] \propto [Cl_g\cdot]^{0.5}$. The ratio of propagation to termination reaction rates should therefore scale as $\sim 1/[Cl_g\cdot]^{0.5}$. From this rough qualitative analysis it is expected that increasing the Cl atom concentration in the gas phase should lead to a decrease in the probability of a secondary chemical reaction in the particle phase. This simple analysis provides a qualitative explanation of the trend shown in Fig. 10, which will be tested quantitatively using the kinetic models described below.

It is also possible that the termination reaction shown in 13a could alternatively occur heterogeneously via the collision of a gas phase $Cl_g\cdot$ atom with a $Cl_p\cdot$ species solvated at particle surface as shown in R13b,

$$Cl_p\cdot + Cl_g\cdot + M \xrightarrow{\gamma_{13}} Cl_{2_p} + M. \quad (13b)$$

For this case, the termination rate should depend upon the reactive collision frequency of $Cl_g\cdot$ with a $Cl_p\cdot$.

In addition to R13, there are two other types of possible termination reactions,

$$R\cdot + R\cdot \xrightarrow{k_{14}} R_2 \quad (R14)$$

$$R\cdot + Cl_p\cdot \xrightarrow{k_{15}} RCl. \quad (R15a)$$

It is difficult to quantify the possible influence of R14 and R15 on the total reaction mechanism, since it would require controlling the concentration of the $R\cdot$ radical experimentally and in a systematic way. In addition, we find no evidence in the mass spectra for the formation of R_2

493 species (e.g. Sq_2) as a reaction product, suggesting that R14 is a minor radical termination
494 channel and therefore neglected in our subsequent analysis. The rate of R15 is roughly
495 proportional to $[Cl_p\cdot]^2$, which is the same dependence observed for R13.

496 As show schematically in Fig. 1, R15 could also occur as a heterogeneous reaction,

497 $$R\cdot + Cl_g\cdot \xrightarrow{\gamma_{15}} RCl, \qquad \text{(R15b)}$$

498 where a surface alkyl radical reacts with a gas phase chlorine atom, thus terminating the radical
499 chain reaction.

500 **C. Kinetic model**

501 Single particle kinetic models that include both heterogeneous and homogeneous
502 reactions are constructed from the set of coupled differential equations corresponding to
503 reactions R2-R7, R13 and R15. Two models, termed "homogeneous" and "heterogeneous" are
504 used, to represent two limiting cases. The first model assumes that the propagation (R3a) and
505 termination pathways (R5a, R13a, and R15a) occur homogeneously inside the particle as
506 shown in Fig. 1. In the second model, the propagation (R3b) and termination (R5b, R13b, and
507 R15b) steps are assumed to proceed heterogeneously at the surface of the particle. The results
508 of the two models are used to predict the measurements of the effective uptake coefficient vs.
509 $[O_2]$, $[Cl_2]$ and [Cl] shown in Figs. 7, 9 and 10.

510 In both models, a single particle size is used to approximate the average diameter of the
511 particle distribution used in each experiment. For the experiments reported here the average
512 diameter is 165-185 nm. The model includes multiple generations of reactions, since Cl atoms
513 can react with both squalane and its various reaction products. RH in R2 represents all closed
514 shell species in the system (e.g. Sq, $SqCl_n$, SqO_n, etc). These species are each allowed to react
515 via the same mechanisms as shown for squalane (R2-R7, R13 and R15). This set of coupled
516 differential equations is solved numerically using an adaptive time step algorithm in
517 *Mathematica*. Although physically unnecessary, 50 generations of products are included in the

model for numerical stability. In this system, there are pure oxygenated and chlorinated products as well as mixed species, making the model extremely complex unless a few simplifying assumptions are made.

First, it is assumed that the primary (i.e. no secondary chemistry) Cl uptake coefficient (γ_{Cl} in R2) is the same for all generations of reaction products (i.e. $\gamma_{Cl}^{Sq} \approx \gamma_{Cl}^{SqCl} \approx \gamma_{Cl}^{SqCl_2} \approx \gamma_{Cl}^{SqCl_3} \approx \gamma_{Cl}^{SqO} \approx \gamma_{Cl}^{SqO_2} \approx \gamma_{Cl}^{SqO_3}$). This was found to be the case for OH + squalane[12] and the Cl + squalane reaction at 20% O_2, as described above. This assumption appears reasonable over the first few generations of reaction products since the addition of only 1-3 functional groups to a C_{30} molecule should not appreciably diminish its overall reactivity toward Cl. Furthermore, this assumption will be verified later when the modeled evolution of the reaction products are directly compared with experiment.

In a similar way, it is also assumed that the rate (R3a) and uptake (R3b) coefficients for Cl_2 reacting with all the alkyl radicals (R·) is the same. The same assumption is made for the rate (R5a) and uptake (R5b) coefficients for the reaction of O_2 with all the various alkyl radicals. The validity of these assumptions will be tested against the observed chlorinated product evolution shown below.

There are few direct measurements of many of the homogenenous or heterogeneous reactions rates for squalane or even long chain hydrocarbons needed to constrain the model using solely previously measured literature values. Therefore, reasonable order of magnitude estimates for the liquid phase rate coefficients can be obtained by estimating the value of a rate coefficient that is limited solely by diffusion in squalane (i.e. zero Arrhenius activation energy). A rate coefficient for a fast reaction, which is only limited by the encounter frequency of two reactants in the liquid (neglecting steric factors) is given by,[32]

$$k_{diff} = 4\pi(D_A + D_B)R \quad (16)$$

where R is the critical radius for reaction and D_A and D_B are the diffusion coefficients for reactants A and B. For spherical particles, the diffusion coefficient is related to viscosity via the

544 Einstein-Stokes relationship,

545 $$D = \frac{k_B T}{6\pi r \eta} \quad (17)$$

546 where k_B is Boltzmann's constant, T temperature, r molecular radii and η, viscosity. For low
547 molecular weight organic solvents such as hexane (η = 0.294 cP),[33] diffusion coefficients are ~
548 10^{-5} cm^2 s^{-1}. Assuming a critical reaction radius of 0.4 nm and a diffusion coefficient of 1 x 10^{-5}
549 cm^2 s^{-1}, liquid phase diffusion limited rate coefficients are on the order of ~1 x 10^{-11} cm^3
550 $molec^{-1}$ s^{-1}. This rate coefficient is about 50 times smaller than the binary collision limited
551 reaction rate constant in the gas phase (~5 x 10^{-10} cm^3 $molec^{-1}$ s^{-1}).

552 Squalane, however, has a viscosity of 17.9 cP,[34] which is 60 times larger than that of
553 hexane. Assuming, a molecular radius of 1 nm (approximated from molecular density of liquid
554 squalane) the diffusion coefficient for squalane is computed to be 1 x 10^{-7} cm^2 s^{-1}, which is
555 reasonably consistent with the range of diffusion coefficients of various solutes[35-36] (0.25-1.4 x
556 10^{-6} cm^2 s^{-1}) in squalane as well as triacontane[37] (7.5 x 10^{-7} cm^2 s^{-1})—the solid straight chain
557 isomer of squalane. Using Eq. (16) the diffusion limited rate coefficient for a reaction occurring
558 in liquid squalane, assuming a critical reaction radius of 0.4 nm, is estimated to be $k_{diff} \approx 10^{-13}$
559 cm^3 $molec^{-1}$ s^{-1}, which is a factor of ~4000 times slower than the gas phase binary collision
560 limit. Given the approximations used above (e.g. a spherical particle in the Einstein-Stokes
561 equation and the molecular radii of squalane) this value serves only as a rough order of
562 magnitude estimate for a diffusion limited rate coefficient in squalane as well as physical basis
563 for the range of condensed phase rate coefficients that will ultimately be used to parameterize
564 the kinetic models.

565 The homogeneous model is first initialized using estimates of the condensed phase rate
566 coefficients for R3a, R4, R5a, R13a and R15a, which is done by slowing down analogous gas
567 phase reactions by the factor of 4000 as described above. For example, the gas phase rate
568 coefficient for the abstraction of a hydrogen atom by Cl from a small alkane is of the order of

569 10^{-10} cm^3 $molec^{-1}$ s^{-1} (e.g. Cl + hexane),[38] which if slowed by a factor of 4000 yields a rough
570 estimate of the condensed phase Cl_p + RH (R3a) rate coefficient of ~10^{-14} cm^3 $molec^{-1}$ s^{-1}.
571 Similarly, the rate coefficient for the reaction of small alkyl radicals (R·) with Cl_2 and O_2 is on
572 the order of 10^{-11} and 10^{-12} cm^3 $molec^{-1}$ s^{-1} respectively.[39] In liquid squalane these rate
573 coefficients are expected to be slowed to ~ 10^{-15} (R3a) and 10^{-16} cm^3 $molec^{-1}$ s^{-1} (R5a),
574 respectively. The radical termination reactions, Cl_p + Cl_p (R13a) and R· + Cl_p (R15a) are
575 assumed to occur at every liquid phase encounter and thus assumed in the model to be diffusion
576 limited (~10^{-13} cm^3 $molec^{-1}$ s^{-1}).[40] These estimates provide a self consistent set of constraints in
577 the model that are used when attempting to replicate the experimental results.
578 To replicate the experimental data using the kinetic model, the Henry's Law constant for
579 O_2 dissolved in squalane is fixed to H_{O2} = 0.18 ($k_{H,cc}$, the dimensionless ratio) as reported in
580 Ref.[41]. To our knowledge the Henry's law constant for Cl_2 dissolved in squalane has not been
581 measured, so an estimate is made using the difference in solubility of O_2 in water and squalane.
582 The Henry's law constant for O_2 in water is 0.03, which is a factor of 6 smaller than that for
583 squalane. The Henry's law constant for Cl_2 in water is measured to be 2,[42] so we estimate that
584 Cl_2 is similarly 6 times more soluable in squalane than in water. So in the model, the Henry's
585 law constant for Cl_2 in squalane is fixed to H_{Cl2} = 12 ($k_{H,cc}$, the dimensionless ratio).
586 As discussed above and shown in Fig. 1, after heterogeneous initiation the subsequent
587 reaction pathways (propagation vs. termination) can proceed either at the surface or within the
588 bulk of the particle. To explore this interplay we first construct a model that considers only
589 homogeneous propagation (R3a) and termination steps (R5a, R13a and R15a). The potential
590 importance of heterogeneous propagation and terminations steps will be discussed below.
591 The Henry's law coefficients for Cl_2 and O_2 are fixed to 12 and 0.18 respectively as
592 described above. The primary Cl uptake coefficient (R2) and the rate coefficients for R3a (R· +
593 Cl_2), R4 (RH + Cl_p·), R5a (R· + O_2), R13a (Cl_p· + Cl_p·) and R15a (R· + Cl_p·) are then adjusted in
594 the model, within the order of magnitude estimates outlined above, to replicate the three sets of

595 experimental results: γ_{Cl}^{Sq} vs. [O_2], [Cl_2], and [Cl] as shown in Figs. 7, 9, and 10. To achieve
596 the best representation of the experimental measurements using the homogeneous model,
597 within the rate constant constraints outlined above, it was found that $\gamma_{Cl} = 0.55$, $k_{3a} = 1.3 \times 10^{-15}$,
598 $k_4 = 1.3 \times 10^{-14}$, $k_{5a} = 8.5 \times 10^{-16}$, and $k_{13a} = k_{15a} = 2.2 \times 10^{-13}$ $cm^3 \cdot molec^{-1} \cdot s^{-1}$.

599 Although the model provides a reasonable description of the experimental results shown
600 in Figs. 7, 9 and 10, care should be exercised in rigorously interpreting the absolute values of
601 the predicted rate coefficients since the kinetic model is highly coupled. For example, the
602 relationship between the effective uptake coefficient and [O_2], shown in Fig. 7, is controlled
603 mainly by the ratio of ($H_{Cl2} \times k_{3a}$) to ($H_{O2} \times k_{5a}$). For the model to replicate the experimental
604 results in Fig. 7, using purely homogeneous propagation and termination pathways this ratio
605 needs to be ~102. In other words, the overall reaction rate of Cl_2 with R· is two orders of
606 magnitude faster than the equivalent reaction with O_2. This can be achieved by a number of
607 combinations of H_{Cl2}, k_{3a}, H_{O2} and k_{5a}.

608 The homogeneous model results, shown as solid lines in Fig. 7, capture the overall
609 functional form of the effective uptake coefficients vs. [O_2] at two fixed Cl_2 concentrations.
610 Both the experimental data and model results show that the large effective uptake coefficients
611 (1.5-3.5) decrease steeply with [O_2] reaching a value of $\gamma_{Cl}^{Sq} = 0.57$, which becomes
612 independent of [O_2] beyond 2%. Unlike the experiment, the modeled effective uptake
613 coefficient can be easily decomposed into contributions from the primary heterogeneous
614 reaction (γ_{Cl}) and secondary chemistry in order to determine chain propagation lengths. The
615 chain propagation length is simply the number of molecules that are removed for each reactive
616 gas phase collision of Cl with the particle (i.e. $\gamma_{Cl}^{Sq}/\gamma_{Cl}$). For example, $\gamma_{Cl}^{Sq} = 0.57$ is very close
617 to the best fit value for the primary reactive uptake coefficient ($\gamma_{Cl} = 0.55$) in the model. This is
618 consistent with our expectation that at high [O_2] the chain terminating pathway (R5a) resulting
619 in stable products such as alcohols and ketones dominates, and therefore the primary
620 heterogeneous reaction controls the overall chemistry rather than the propagating reaction (R·

621 + Cl_2). Alternatively, at low [O_2] (and [Cl_2] = 32.7 ppm) secondary reactions dominate, with
622 radical chain lengths as large as 6.3 (3.5/0.55), indicating that for each molecule in the particle
623 consumed by the heterogeneous reaction six others are removed via secondary reactions.

624 Shown in Fig. 9 are measurements of the effective uptake coefficients as a function of Cl_2
625 concentration. These measurements are intended to isolate, to the extent possible, how the
626 reaction scheme depends upon absolute Cl_2 concentration. Completely isolating the Cl_2
627 dependence experimentally from the inverse dependence of the effective uptake coefficient on
628 [Cl], shown in Fig. 10, is difficult since the measurements of effective uptake coefficients
629 shown in Fig. 9 are made by varying the average [Cl] at a fixed concentration of Cl_2. For
630 example, the uptake coefficient measurement at [Cl_2] = 7 ppm requires a larger average
631 concentration of chlorine atoms ($\langle Cl \rangle_t$ = 1x10^{10} molec/cm^3) than the measurement at [Cl_2] = 30
632 ppm ($\langle Cl \rangle_t$= 1x10^9 molec/cm^3) to obtain a decay trace ([Sq]/[Sq]$_0$ vs. Cl exposure) of sufficient
633 length for the accurate determination of the kinetic decay constant used to compute an uptake
634 coefficient. This is because at lower [Cl_2] the reaction occurs ~3 times slower than at [Cl_2] = 30
635 ppm, thus requiring higher $\langle Cl \rangle_t$ in the former case. Consequently, for these sets of
636 measurements, the kinetic model is used to simulate each data point using the average Cl atom
637 and Cl_2 concentrations used in the experiment. In this way, modeled decay curves can be
638 generated that resemble the experimental measurements shown in Fig. 6. These modeled decay
639 curves are then fit to single exponential functions to extract the modeled uptake coefficients
640 shown in Fig. 9. The homogeneous model results are shown as solid lines in Fig. 9 and reveal,
641 as does the experimental data, that the effective uptake coefficient monotonically increases
642 with [Cl_2]. At low [Cl_2] the effective uptake coefficient approaches the primary heterogeneous
643 reaction probability (γ_{Cl} = 0.55) and increases to γ_{Cl}^{Sq} = ~3 at [Cl_2] = 32 ppm, which
644 corresponds to a chain propagation length of ~6.

645 In Fig. 10, the model captures the experimentally determined effective uptake coefficients
646 as a function of [Cl]. Unfortunately, experimental limitations prevent measurements at Cl

concentrations in excess of 2 x 10^{10} molec/cm^3. Nevertheless the model shows that the effective uptake coefficient approaches 0.55 in the limit of high [Cl], which as discussed above is the primary heterogeneous reaction probability (γ_{Cl} = 0.55). Under these conditions, radical chain lengths of 3.54 and 1.54 at [Cl] = 2.67 x 10^9 molec cm^{-3} and 2.2 x 10^{10} molec cm^{-3} are observed, respectively.

The kinetic model, parameterized with purely homogeneous propagation and termination pathways, correctly describes how the measured effective uptake coefficient depends upon [Cl_2], [O_2] and [Cl]. Although, the evolution of oxygenated products, in the absence of secondary chemistry, discussed in Section III.A, is well described by a sequential oxidation model whose analytical form is shown in Eq. (12), it should be noted that the numerical kinetic model, described above, also correctly predicts the chemical evolution of oxygenated reaction products at 20% O_2 observed in Fig. 8.

As shown in Fig. 1, the propagation and terminal reaction pathways can also proceed at the surface via collisions with gas phase species such as Cl_2, O_2 and Cl. To evaluate the potential importance of these surface pathways the overall rate of the R· + Cl_2 and R· + O_2 heterogeneous reactions are compared with the analogous reactions occurring within the particle. For the homogeneous R· + Cl_2 propagation reaction the time dependent change in concentration of R· is given by,

$$\frac{d[R\cdot]}{dt} = k_{3a}[Cl_2]H_{Cl2}[R\cdot] = (1.6 \times 10^{-14})\,[Cl_2][R\cdot]\,s^{-1} \quad (18)$$

which can be compared to the equivalent expression for the heterogeneous reaction,

$$\frac{d[R\cdot]}{dt} = \frac{\gamma_{Cl2}\,\overline{c}_{Cl2}\,A\,[Cl_2][R\cdot]}{4\;Sq_0V} = \frac{(3.9\times10^{-17})\,\gamma_{Cl2}[Cl_2][R\cdot]s^{-1}}{d} \quad (19)$$

where V, A and d are the particle volume, surface area and diameter respectively. $\overline{c}_{Cl2}$ is the mean speed of Cl_2, and Sq_0 is the molecular density of squalane. It should be noted that Eq. (19) assumes that the particle is well mixed on the time scale of the reaction, as previously shown by Smith et al.[12] For the average diameter (167 nm) used in the experiments reported here,

672 dividing the heterogeneous (Eq. (19)) by the homogeneous (Eq. (18)) rate yields,

673 $$\frac{Hetero.}{Homo.} = 151\,\gamma_{Cl2} \quad (20)$$

674 thus providing a measure of the competition between the heterogeneous and homogeneous R· +
675 Cl_2 reaction pathways. If the heterogeneous reaction occurs with every collision of a gas phase
676 Cl_2 molecule with an molecule containing an alkyl radical at the particle surface (i.e. $\gamma_{Cl2} = 1$),
677 then the heterogeneous propagation rate, for the particle sizes used here, is over two orders of
678 magnitude faster than the equivalent reaction of dissolved Cl_2 with R· inside the particle.
679 However, if it is assumed that there is on average only 1 radical site per molecule then the
680 uptake coefficient is therefore likely to be much less than one. For example, there are 62
681 hydrogen atoms in squalane yielding 62 possible locations for the formation of R·. In this case,
682 a more reasonable value for γ_{Cl2} is 1/62 or 0.016, which suggests that the heterogeneous
683 reaction is only faster by a factor of 2.4.

684 The same analysis can be applied to the R· + O_2 reaction to evaluate its potential
685 importance at the surface of the particle. In this case, the ratio is,

686 $$\frac{Hetero.}{Homo.} = 22705\,\gamma_{O2} \quad (21)$$

687 suggesting that there is a much larger possible heterogeneous contribution to this reaction
688 pathway for the particle sizes investigated here. For the heterogeneous and homogeneous rates
689 to be equal, γ_{O2} would be on the order of 10^{-5}. Such a straightforward comparison of the R· +
690 Cl and Cl + Cl termination reactions is difficult, but it was determined that even if the uptake
691 coefficient for these reactions were in fact unity, there would be less than a 0.5% change in the
692 homogeneous model results presented above and shown in Fig. 7, 9 and 10. This then suggests
693 that these radical-radical termination reactions occur primarily as homogeneous reactions
694 inside the particle. Consequently, these heterogeneous termination reactions (R13b and R15b)
695 are neglected in the model that is presented below.

696 The preceding analysis therefore suggests that, for the average particle sized used here, the

heterogeneous propagation ($R\cdot + Cl_2$) and termination ($R\cdot + O_2$) might play a significant role in the observed kinetics. To illustrate this possibility, a purely heterogeneous model is constructed, the results of which are plotted as dotted lines in Fig. 7, 9 and 10. In this case, we assume the primary uptake coefficient for Cl_g is 0.55, and the rate coefficient k_4 = 1.3 x 10^{-14} $cm^3 \cdot molec^{-1} \cdot s^{-1}$ ($RH + Cl_p$) and $k_{13a} = k_{15a}$ = 2.2 $\times 10^{-13}$ $cm^3 \cdot molec^{-1} \cdot s^{-1}$, which are the same values used in the homogeneous model described above. The experimental data shown in Figs. 7, 9, and 10 can be well represented by the purely heterogeneous model using the following parameters: γ_{Cl2} = 0.01 and γ_{O2} = 5 x 10^{-5}. These uptake coefficients indicate that for Cl_2 nearly every collision with a radical site (1 site per molecule with 62 possible sites) yields a reaction, while for O_2 1 in every 320 collisions with the radical site yields a reaction. Since the model is highly coupled and heterogeneous measurements of $R\cdot + O_2$ and $R\cdot + Cl_2$ reaction probabilities have not been previously quantified, caution again should be exercised in interpreting any of the absolute values of the uptake coefficients reported here. Nevertheless, to reproduce the experimental data the heterogeneous rate of $R\cdot + Cl_2$ is found to be 130 times larger than the $R\cdot + O_2$ uptake coefficient. This is similar in magnitude to the differences homogeneous rates for the same reactions described above.

Unfortunately, the measured data set is insufficient to fully ascertain what fraction of the measured effective uptake coefficient originates from the heterogeneous vs. homogeneous reaction pathways. However, it seems likely, given the model results for the rate and uptake coefficients used here, that indeed both reaction pathways are competitive. One large factor is the slowing of the homogeneous reaction pathways by the viscosity of squalane. To distinguish between these heterogeneous and homogeneous process would require further experimental constraints of various rate and uptake coefficients, for the $R\cdot + Cl_2$ and $R\cdot + O_2$ reactions. Furthermore, the heterogeneous reaction mechanism is expected to increase in importance as the average size of the particle distribution is decreased (see Eq. (19)), since for smaller particles there will be on average a larger fraction of surface alkyl radicals (assuming a well

mixed particle) available for a heterogeneous reaction with O_2 or Cl_2. Therefore, systematic studies, such as those described here could be extended to size-selected particles with broad range of diameters to potentially constrain the relative importance of the heterogeneous and homogeneous reaction pathways.

To further understand generally, how secondary chemistry impacts the evolution of reaction products, both models will be used to predict the kinetic evolution of chlorinated products formed at low [O_2] concentrations as described below.

D. The formation and evolution of chlorinated reaction products

Chlorinated reaction products, formed at low [O_2], are observed in the mass spectra as shown in Figs. 4 and 5. The product ion peaks in the mass spectrum that evolve as a function of chlorine exposure are labeled SqCl′ (*m/z* = 454), $SqCl_2'$ (*m/z* = 488), and $SqCl_3'$ (*m/z* = 522), as shown in Fig. 11. This series of peaks correspond to products in which H atom(s) are replaced with Cl atom(s). There is one main product ion (Sq-2′) at *m/z* = 420, which is 2 mass units smaller than that of squalane and could correspond to the formation of a stable alkene molecule, although it is difficult to rationalize the formation of this product given the well-established low temperature hydrogen abstraction mechanisms. To determine if this product does indeed correspond to an alkene, the particle stream was directed into a second flow tube containing ozone (~5.1 ppm for ~1 min.). Since ozone reacts quickly with alkenes, a change in the particle phase composition is expected if alkenes are indeed formed as reaction products. However, we find no evidence that the particle reacts with ozone.

A more probable explanation for these peaks in the mass spectrum is dissociative photoionization of $SqCl_n$, which eliminates HCl. For smaller chlorinated hydrocarbons, such as 1-chloro-pentane, HCl elimination upon photoionization is a significant dissociation pathway.[38, 43-44] Furthermore, the electron impact mass spectra of small chlorinated hydrocarbons produces hydrocarbon fragments consistent with HCl elimination, providing further evidence for this channel.[38] It is therefore extremely likely that a similar dissociative

749 photoionization pathway is occurring for the chlorinated hydrocarbons observed here. In this
750 case, the Sq-2′ peak forms from the elimination of HCl from the $SqCl^+$ ion, (*m/z* = 456-36 = 420
751 = Sq-2′), $SqCl'^+$ from $SqCl_2^+$ (*m/z* = 490-36 = 454 = Sq-2′+34), $SqCl_2'^+$ from $SqCl_3^+$, (*m/z* =
752 524-36 = 488 = Sq-2′+34+34) and so on.

753 The chemical evolution of the particle is shown in Fig. 11. This figure shows how squalane
754 and four generations of chlorinated products, at low O_2, evolve as a function of chlorine
755 exposure. Each product is both formed and decays over the course of the reaction. The arrows
756 in Fig. 11 indicate the Cl exposures that correspond to 1, 2, 3, and 4 squalane lifetimes ($\tau = 1/k_{Sq}$), respectively. Unlike the kinetic evolution of the oxygenated products (at 20% O_2) shown
758 in Fig. 8, there is no longer a simple relationship between squalane lifetimes and the peak
759 maxima in the kinetic evolution of each reaction product. For the 20% O_2 case, the maxima in
760 the evolution of SqO_n products as a function of Cl exposure are equally spaced and coincide
761 with n squalane lifetimes. While the first chlorinated reaction product SqCl (detected as *m/z* =
762 Sq-2') reaches its maxima around 1 squalane lifetime, similar to the kinetic evolution of SqO,
763 subsequent generations of chlorine products reach their maxima at much larger lifetimes than
764 predicted by the sequential model (Eq. (12)). In fact, the deviation of the product evolution
765 from the sequential oxidation model (Eq. (12)) becomes larger for each subsequent generation
766 of chlorinated reaction product.

767 Results from the kinetic models (described in Sec. III.C) are used to simulate the product
768 evolution as shown in Fig. 11. The models are parameterized to replicate the experimental
769 conditions by fixing the reaction time and changing the Cl exposure via increasing (or
770 decreasing) the chlorine atom concentration. The same set of rate and uptake coefficients are
771 used to model the reaction products that were previously used to achieve the best
772 representation of effective uptake measurements shown in Figs. 7, 9, and 10. This not only
773 provides an additional test of the overall chemistry included in the kinetic models, but provides
774 a global view of both the reaction rate (effective uptake coefficients) and the chemical

775 evolution of the particle undergoing significant amounts of radical chain chemistry. As
776 discussed above, all of the homogeneous rate and heterogeneous uptake coefficients for all
777 generations of products ($SqCl_n$) are assumed to be the same.

778 Shown as solid lines in Fig. 11, the homogeneous model can capture the overall evolution
779 of the first four chlorinated reaction products at both ~0% and 0.14 % O_2 (Cl_2 = 32.7 ppm). For
780 comparison the heterogeneous model predictions are shown as dotted lines in Fig. 11. For both
781 models there are some discrepancies between predictions and the experimental. These
782 deviations between the models and the experimental data may arise from slightly non-uniform
783 concentrations of Cl along the length of the flow reactor, which would not be properly
784 accounted for in the model since a single average [Cl] for the whole flow tube is used to
785 generate the model lines shown in Fig. 11.

786 Nevertheless, the overall rate and chemical evolution of the particle is well-represented by
787 both the homogeneous and heterogeneous kinetic models and reveals that, in this system,
788 which is dominated by radical chain chemistry, the formation of reaction products evolve in a
789 more complex way than for the OH + squalane reaction or the Cl + squalane reaction at 20% O_2.
790 The agreement between model and experiment also reveals that, within measurement error and
791 over the first couple of generations of reaction, both the chemistry of squalane and its
792 subsequent reaction products can indeed be approximated by a single rate and uptake
793 coefficients (e.g. $\gamma_{Cl}^{Sq} \approx \gamma_{Cl}^{SqCl} \approx \gamma_{Cl}^{SqCl_2} \approx \gamma_{Cl}^{SqCl_3} \approx \gamma_{Cl}^{SqO} \approx \gamma_{Cl}^{SqO_2} \approx \gamma_{Cl}^{SqO_3}$).

794 The difference between the measured kinetic evolution of reaction products at low and 20 %
795 O_2 is a natural consequence of radical chain chemistry. The product kinetics, shown in Fig. 11,
796 are measured by increasing the concentration of chlorine atoms in the flow tube. However, as
797 shown in Fig. 10, the effective uptake coefficient decreases with increasing chlorine atom
798 concentration. The inverse dependence of the effective uptake coefficient on [Cl] is discussed
799 above and originates from the increasing importance of reactions such as R13 and R15, the $Cl\cdot_p$
800 + $Cl\cdot_p$ and $R\cdot$ + $Cl\cdot_p$ chain termination reactions, at high Cl concentrations. These reactions have

801 the net consequence of decreasing the overall radical propagation length (i.e. the amount of
802 secondary chemistry) in the particle phase as the [Cl] increases and the reaction progresses.
803 This interplay between radical propagation and termination has the net consequence of slowing
804 down the reaction at larger chlorine exposures. This in turn modifies the kinetic evolution of
805 the chlorinated reaction products, whose chemical evolution increasingly deviates from that
806 observed for the oxygenated products formed at 20 % O_2.

807 Finally, it should also be pointed out that the presence of secondary chemistry, as observed
808 here, produces kinetics in which reaction time and concentration (i.e. [Cl_g·]) are not longer
809 interchangeable quantities. For example, measurements that only change reaction time at a
810 fixed [Cl_g·] will produce quite different results from those experiments that fix reaction time
811 and scan [Cl_g·], which is consistent with observations reported by McNeil et al.[8]

812 **IV. Conclusion**

813 The heterogeneous reaction of squalane with Cl atoms is examined using VUV
814 photoionization aerosol mass spectrometry. In the absence of O_2, chlorinated reaction products
815 are formed and a radical chain reaction is observed; propagated by the R· + Cl_2 → RCl + Cl·
816 reaction. Effective uptake coefficients vary from 0.8 to ~3 and correspond to radical chain
817 propagation lengths of 1.4 and ~6, respectively. The magnitude of the effective uptake
818 coefficient is found to be directly proportional to the [Cl_2] in the flow reactor. Furthermore, it
819 was found that the effective uptake coefficient is inversely proportional to [Cl]. This inverse
820 correlation arises from the competitive rates of chain propagation and termination.

821 Adding as much as 20% O_2 to the reaction, effectively shuts off the chain cycling reaction,
822 produces oxygenated products and decreases the uptake coefficient to ~0.57. The
823 diffusion-corrected uptake coefficient is found to be 0.65±0.07 and the chemical evolution of
824 the particle follows a sequential oxidation mechanism. Under these conditions the Cl initiated
825 oxidation of the particle is nearly identical to that found for the OH + squalane reaction albeit
826 ~2.2 times faster, due to the larger initial reactive uptake coefficient.

827 Two detailed kinetic models are formulated to explore two limiting cases: homogeneous
828 vs. heterogeneous chain propagation and termination. Both models provide a reasonable and
829 independent representation of the global data set, which accounts for how the effective uptake
830 coefficients and product evolutions depend upon $[Cl_2]$, [Cl] and $[O_2]$. As a result, it is not easy
831 to evaluate the relative importance of each pathway on the global mechanism. However, the
832 results presented here suggest that for radical reactions in viscous droplets, such as squalane,
833 the slow diffusion of reactants inside the particle may enhance the potential importance of
834 competing heterogeneous reaction pathways.
835 These results clearly illustrate, in a more general way, that for heterogeneous reactions in
836 which free radical intermediates propagate chain reactions, time and concentration, generally
837 considered in aggregate as exposure, are no longer independent separable kinetic quantities.
838 As a consequence, the reaction probability and product evolution will be markedly different if
839 measured as a function of time and therefore may not be directly comparable to those
840 measurement that change radical exposure by concentration. The observation and easy control
841 of secondary chemistry in this system could be used to further explore how molecular structure
842 (n-alkane vs. branched alkane, alkane vs. alkene) might control radical chain reaction
843 chemistries.

844 **Acknowledgements**

845 This work was supported by the Director, Office of Energy Research, Office of Basic Energy
846 Sciences, Chemical Sciences Division of the U.S. Department of Energy under Contract No.
847 DE-AC02-05CH11231. C.L.L. is partly supported by the National Science Council, Taiwan
848 under Contract NO. NSC97-2917-I-564-142. J.D.S. was partially supported by the Camille and
849 Henry Dreyfus foundation postdoctoral program in environmental chemistry during this work.
850 D.L.C. is grateful to the National Aeronautics and Space Administration for support on Grant
851 NASA-NNG06GGF26G.

852

853 **References**

854 1. S. M. Aschmann and R. Atkinson, *Int. J. Chem. Kinet.*, 1995, **27**, 613-622.

855 2. E. S. C. Kwok and R. Atkinson, *Atmos. Environ.*, 1995, **29**, 1685-1695.

856 3. C. W. Spicer, E. G. Chapman, B. J. Finlayson-Pitts, R. A. Plastridge, J. M. Hubbe, J. D.
857 Fast and C. M. Berkowitz, *Nature*, 1998, **394**, 353-356.

858 4. K. W. Oum, M. J. Lakin, D. O. DeHaan, T. Brauers and B. J. Finlayson-Pitts, *Science*,
859 1998, **279**, 74-77.

860 5. J. P. Kercher, T. P. Riedel and J. A. Thornton, *Atmos. Mears. Tech.*, 2009, **2**, 193-204.

861 6. J. D. Hearn and G. D. Smith, *Geophys. Res. Lett.*, 2006, **33**.

862 7. J. D. Hearn, L. H. Renbaum, X. Wang and G. D. Smith, *Phys. Chem. Chem. Phys.*, 2007,
863 **9**, 4803-4813.

864 8. V. F. McNeill, R. L. N. Yatavelli, J. A. Thornton, C. B. Stipe and O. Landgrebe, *Atmos.*
865 *Chem. Phys.*, 2008, **8**, 5465-5476.

866 9. I. J. George, A. Vlasenko, J. G. Slowik, K. Broekhuizen and J. P. D. Abbatt, *Atmos.*
867 *Chem. Phys.*, 2007, **7**, 4187-4201.

868 10. E. A. Weitkamp, A. T. Lambe, N. M. Donahue and A. L. Robinson, *Environ. Sci.*
869 *Technol.*, 2008, **42**, 7950-7956.

870 11. A. T. Lambe, M. A. Miracolo, C. J. Hennigan, A. L. Robinson and N. M. Donahue,
871 *Environ. Sci. Technol.*, 2009, **43**, 8794-8800.

872 12. J. D. Smith, J. H. Kroll, C. D. Cappa, D. L. Che, C. L. Liu, M. Ahmed, S. R. Leone, D.
873 R. Worsnop and K. R. Wilson, *Atmos. Chem. Phys.*, 2009, **9**, 3209-3222.

874 13. P. D. Lightfoot, R. A. Cox, J. N. Crowley, M. Destriau, G. D. Hayman, M. E. Jenkin, G.
875 K. Moortgat and F. Zabel, *Atmospheric Environment Part a-General Topics*, 1992, **26**,
876 1805-1961.

877 14. G. S. Tyndall, R. A. Cox, C. Granier, R. Lesclaux, G. K. Moortgat, M. J. Pilling, A. R.
878 Ravishankara and T. J. Wallington, *J. Geophys. Res.-Atmos.*, 2001, **106**, 12157-12182.

15. K. S. Docherty and P. J. Ziemann, *J. Phys. Chem. A*, 2006, **110**, 3567-3577.

16. J. E. Bennett and R. Summers, *Can. J. Chem.-Rev. Can. Chim.*, 1974, **52**, 1377-1379.

17. K. U. Ingold, *Accounts Chem. Res.*, 1969, **2**, 1-&.

18. G. A. Russell, *J. Am. Chem. Soc.*, 1957, **79**, 2977-2978.

19. E. T. Denisov and I. B. Afanan'ev, *Oxidation and Antioxidants in Organic Chemistry and Biology*, Taylor & Francis Group, NW, 2005.

20. T. Moise and Y. Rudich, *Geophys. Res. Lett.*, 2001, **28**, 4083-4086.

21. Z. Zhao, D. T. Huskey, J. M. Nicovich and P. H. Wine, *Int. J. Chem. Kinet.*, 2008, **40**, 259-267.

22. E. Gloaguen, E. R. Mysak, S. R. Leone, M. Ahmed and K. R. Wilson, *Int. J. Mass Spectrom.*, 2006, **258**, 74-85.

23. D. L. Che, J. D. Smith, S. R. Leone, M. Ahmed and K. R. Wilson, *Phys. Chem. Chem. Phys.*, 2009, **11**, 7885-7895.

24. N. A. Fuchs and A. G. Sutugin, *Highly Dispersed Aerosols*, Ann Arbor Science Publishers, Ann Arbor, 1970.

25. D. R. Hanson, A. R. Ravishankara and E. R. Lovejoy, *J. Geophys. Res.-Atmos.*, 1996, **101**, 9063-9069.

26. J. C. Andre, J. Y. Jezequel, R. H. Clark and D. Husain, *Journal of Photochemistry*, 1980, **14**, 245-251.

27. C. J. Hwang, R. C. Jiang and T. M. Su, *J. Chem. Phys.*, 1986, **84**, 5095-5101.

28. A. V. Ivanov, S. Trakhtenberg, A. K. Bertram, Y. M. Gershenzon and M. J. Molina, *J. Phys. Chem. A*, 2007, **111**, 1632-1637.

29. P. A. J. Bagot, C. Waring, M. L. Costen and K. G. McKendrick, *J. Phys. Chem. C*, 2008, **112**, 10868-10877.

30. G. M. Nathanson, *Annu. Rev. Phys. Chem.*, 2004, **55**, 231-255.

31. D. J. Garton, T. K. Minton, M. Alagia, N. Balucani, P. Casavecchia and G. G. Volpi, *J.*

Chem. Phys., 2000, **112**, 5975-5984.

32. J. I. Steinfeld, J. S. Francisco and W. L. Hase, *Chemical Kinetics and Dynamics*, Prentice Hall, New Jersey, 1989.

33. L. H. Luthjens, H. C. Deleng, J. M. Warman and A. Hummel, *Radiat. Phys. Chem.*, 1990, **36**, 779-784.

34. C. F. Poole, R. M. Pomaville and T. A. Dean, *Anal. Chim. Acta*, 1989, **225**, 193-203.

35. A. F. Olea and J. K. Thomas, *J. Am. Chem. Soc.*, 1988, **110**, 4494-4502.

36. I. A. Shkrob, M. C. Sauer and A. D. Trifunac, *J. Phys. Chem.*, 1996, **100**, 5993-6002.

37. T. Vardag, N. Karger and H. D. Ludemann, *Ber. Bunsen-Ges. Phys. Chem. Chem. Phys.*, 1991, **95**, 859-865.

38. Webbook, The National Institute of Standards and Technology (NIST) Gaithersburg, MD.

39. E. G. Estupinan, S. J. Klippenstein and C. A. Taatjes, *J. Phys. Chem. B*, 2005, **109**, 8374-8387.

40. J. A. M. Simoes, A. Greenberg and J. F. Liebman, eds., *Energetics of Organic Free Radicals*, Blackie Academic and Professional, Glasgow, 1996.

41. S. V. Vasenkov, V. A. Bagryansky, V. V. Korolev and V. A. Tolkatchev, *Radiat. Phys. Chem.*, 1991, **38**, 191-197.

42. W. P. Bartlett and D. W. Margerum, *Environ. Sci. Technol.*, 1999, **33**, 3410-3414.

43. D. Harnish, J. L. Holmes, F. P. Lossing, A. A. Mommers, A. Maccoll and M. N. Mruzek, *Org. Mass Spectrom.*, 1990, **25**, 381-385.

44. Y. R. Luo and P. D. Pacey, *Int. J. Mass Spectrom. Ion Process.*, 1992, **112**, 63-77.

930 **Figure captions**

931 Figure 1. An schematic of the potential reaction mechanism initiated by the heterogeneous
932 reaction of Cl atoms with squalane particles in the presence of O_2 and Cl_2. Both heterogeneous
933 and homogeneous propagation and termination reaction pathways are shown separately.
934
935 Figure 2. Schematic of the photochemical flow reactor. The total flow rate through the reactor
936 is 1.1 L/min and corresponds to a reaction time of 33.5 seconds. Chlorine atoms are formed via
937 the photolysis of Cl_2 at 365 nm using black lights (BLB). The photon flux is adjustable using a
938 variac. After reaction, the gas stream is sampled by a SMPS (TSI model 3936), VUV-AMS,
939 and GC for measurements of the particle size distribution, aerosol composition, and Cl
940 exposure, respectively.
941
942 Figure 3. Cl exposure as a function of illumination length at $[Cl_2]$ = 8 ppm. It is found that Cl
943 exposure is linearly proportional to illuminated length (i.e. Cl atom concentration is constant)
944 only for illumination lengths greater than 33 cm.
945
946 Figure 4. 10 eV photoionization mass spectra of squalane aerosol. (a) Before reaction, the main
947 peaks observed in the spectrum are the squalane molecular ion (*m/z* = 422) and its largest
948 fragment ion (*m/z* = 238). (b), (c) After reaction with Cl atoms (32 ppm Cl_2 and 0.143% O_2.),
949 there are a series of product ion peaks (*m/z* > 422), each separated by 34 amu. The peaks,
950 labeled Sq-2′, SqCl′, $SqCl_2$′ and $SqCl_3$′, are formed via dissociative photoionization (i.e. HCl
951 elimination) of $SqCl^+$, $SqCl_2^+$, $SqCl_3^+$, and $SqCl_4^+$ ions, respectively, as discussed in Sec. III.D.
952 Oxygenated reaction products are separated by 14 mass units. There are also peaks in the mass
953 spectra that correspond to mixed products species that contain both oxygen and chlorine
954 functional groups.
955

Figure 5. 10 eV photoionization mass spectra recorded at $[Cl_2]$ = 32.7 ppm and $[O_2]$ = (a) ~0%; (b) 0.3%; (c) 1%; (d) 5%. The peaks identified with dashed lines are second and third generation (n) chlorinated reaction products, denoted as $SqCl_{n-1}'$ originating from $SqCl_n$ as detailed in the text. At low $[O_2]$, only chlorinated products are observed. The chlorinated product peaks decrease and the oxygenated products (i.e. SqO_n) increase with $[O_2]$. When $[O_2]$ is larger than 5%, only oxygenated products are observed.

Figure 6. Normalized kinetic decay of squalane measured as a function of Cl exposure at 14.5 ppm chlorine for (•) $[O_2]$ = 20% and (○) $[O_2] \leq 0.2$ %. Both decay curves are fit using single exponential functions (solid lines).

Figure 7. Effective reactive uptake coefficients as a function of $[O_2]$ at $[Cl_2]$ = (a) 14.5 ppm and (b) 32.7 ppm. Solid lines are predictions from the kinetic model parameterized with homogeneous propagation reactions as detailed in Sec. III.C. Dotted lines are predictions from the heterogeneous kinetic model also detailed in Sec. III.C.

Figure 8. The evolution of squalane (Sq) and its first three generations of reaction products (SqO, SqO_2, SqO_3) as a function of chlorine exposure at $[O_2]$ = 20% and $[Cl_2]$ = 24.6 ppm. Solid lines are results of a sequential oxidation model (Eq. (12)) described in Sec. III.A. The arrows in panels (b), (c) and (d) indicate the chlorine exposures that correspond to 1, 2, and 3 squalane lifetimes, respectively, as described in the text.

Figure 9. Effective reactive uptake coefficients as a function of $[Cl_2]$. The experimental data (○) exhibits a linear increase with $[Cl_2]$. Both the homogeneous (solid lines) and heterogeneous (dotted lines) models predict the same linear increase in effective uptake coefficient with increasing $[Cl_2]$.

Figure 10. Effective uptake coefficients as a function of [Cl] at [Cl_2] = 14.5 ppm shown with the results of the homogeneous (solid lines) and heterogeneous (dotted lines) model predictions.

Figure 11. The evolution of squalane (Sq) and the first four generations ($SqCl_n$) of reaction products as a function of chlorine exposure at [Cl_2] = 32.7 ppm. For (a) to (e) [O_2] = ~0.02% and (f) to (j) [O_2] = 0.14%. The chlorinated reaction products, denoted as $SqCl_{n-1}'$ originate from $SqCl_n$ as detailed in the Sec. III.D. Results from the homogeneous (solid lines) and heterogeneous (dotted lines) models are computed at each experimental point using the average chlorine concentration ($\langle Cl \rangle_t$). The arrows shown in (b) and (g) correspond to 1 squalane lifetime, while the arrows in (c) and (h), (d) and (i), and (e) and (j) indicate the chlorine exposures that correspond to 2, 3, and 4 squalane lifetimes, respectively.

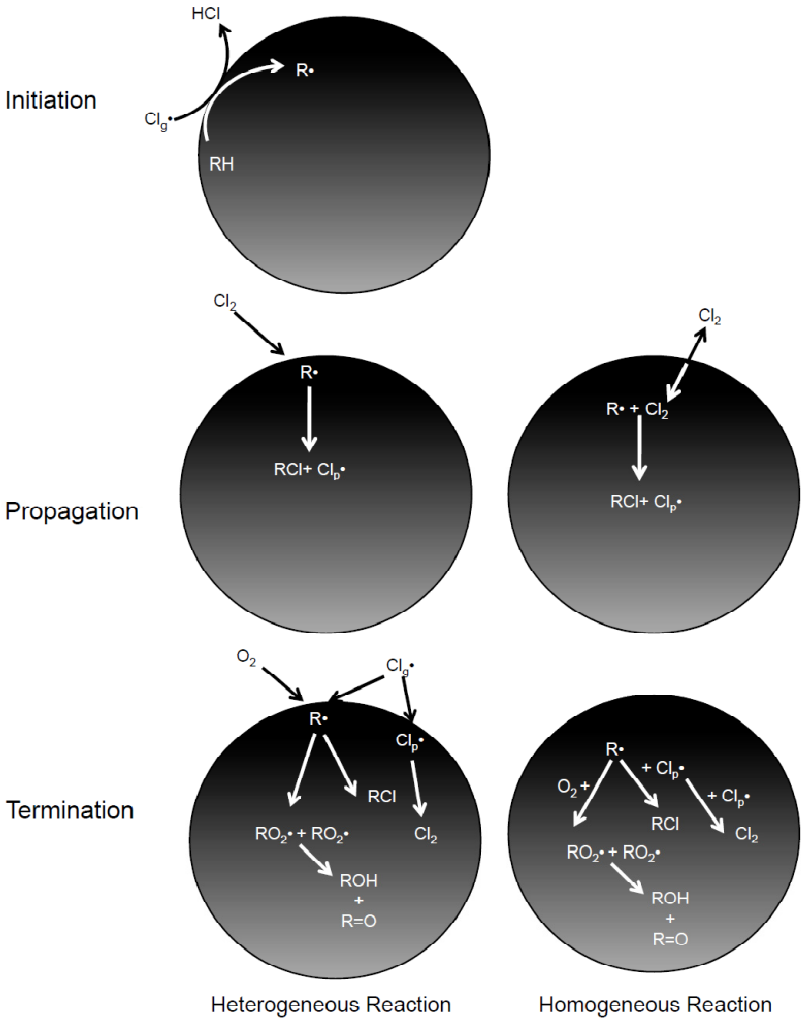
Initiation
HCl
R•
Cl_g•
RH
Propagation
Cl_2
R•
RCl+ Cl_p•
Cl_2
R• + Cl_2
RCl+ Cl_p•
Termination
O_2
Cl_g•
R•
Cl_p•
RCl
RO_2• + RO_2•
Cl_2
ROH
+
R=O
R•
+ Cl_p•
O_2 +
+ Cl_p•
RCl
Cl_2
RO_2• + RO_2•
ROH
+
R=O
Heterogeneous Reaction
Homogeneous Reaction

Figure 1

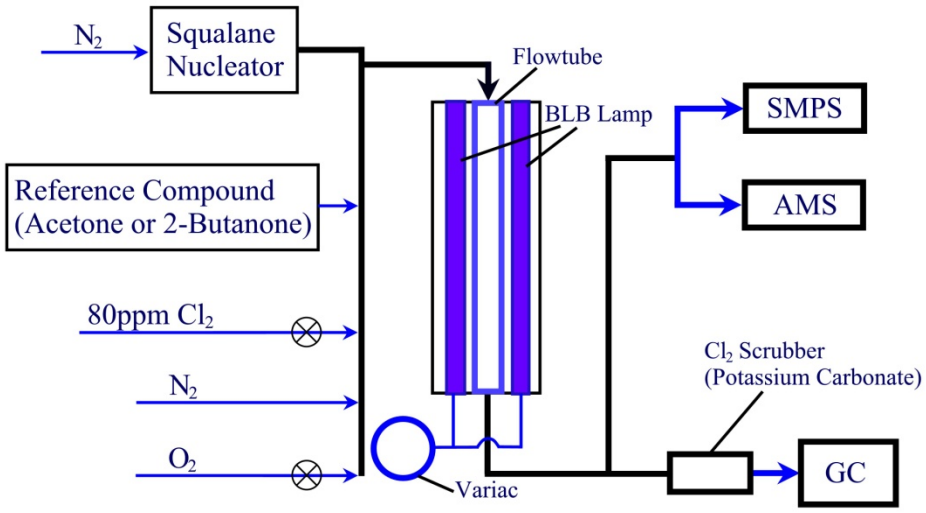
N_2
Squalane Nucleator
Flowtube
BLB Lamp
SMPS
AMS
Reference Compound (Acetone or 2-Butanone)
80ppm Cl_2
N_2
O_2
Variac
Cl_2 Scrubber (Potassium Carbonate)
GC

Figure 2

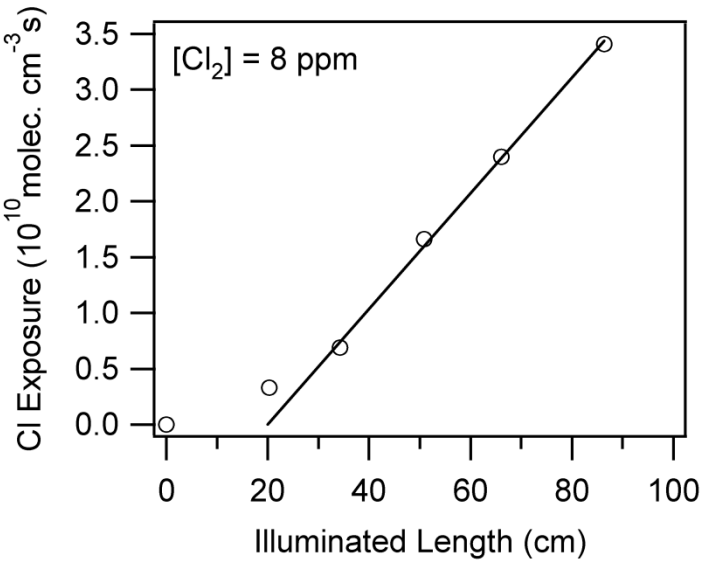
[Cl2] = 8 ppm
Cl Exposure (10^10 molec. cm^-3 s)
Illuminated Length (cm)
0.0
0.5
1.0
1.5
2.0
2.5
3.0
3.5
0
20
40
60
80
100

Figure 3

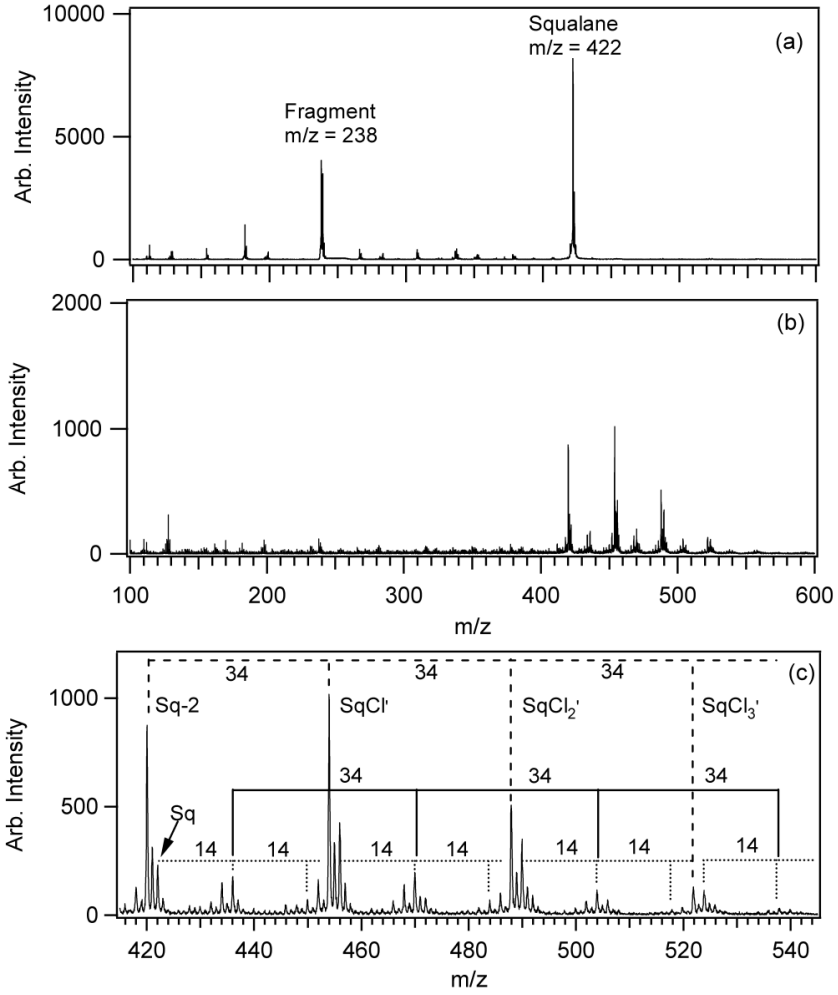
Squalane
m/z = 422
(a)
Fragment
m/z = 238
Arb. Intensity
10000
5000
0
(b)
2000
1000
0
100
200
300
400
500
600
m/z
(c)
34
Sq-2
SqCl'
SqCl2'
SqCl3'
Sq
14
1000
500
0
420
440
460
480
500
520
540

Figure 4

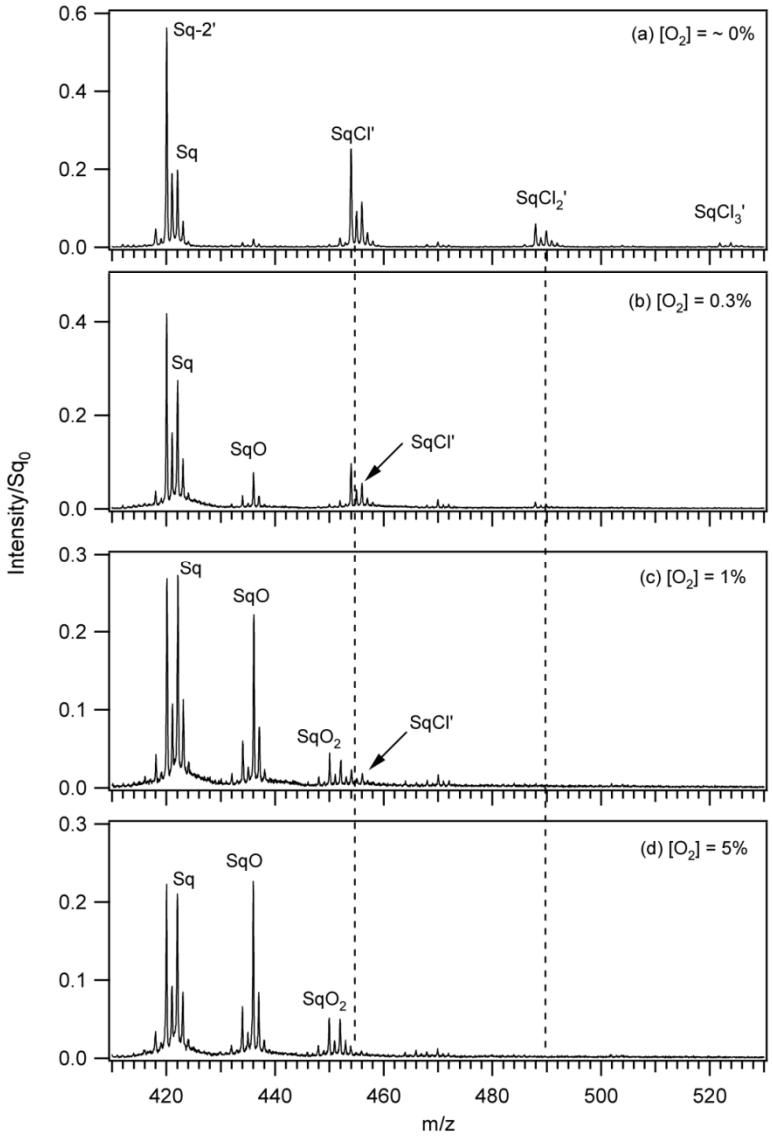
Intensity/Sq0
m/z
(a) [O2] = ~ 0%
(b) [O2] = 0.3%
(c) [O2] = 1%
(d) [O2] = 5%
Sq-2'
Sq
SqCl'
SqCl2'
SqCl3'
SqO
SqO2
0.0
0.1
0.2
0.3
0.4
0.6
420
440
460
480
500
520

Figure 5

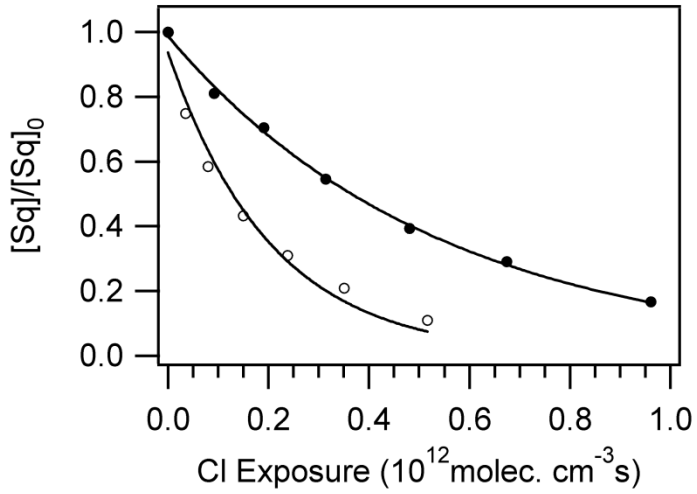
1.0
0.8
0.6
0.4
0.2
0.0
[Sq]/[Sq]0
0.0
0.2
0.4
0.6
0.8
1.0
Cl Exposure (10^12 molec. cm^-3 s)

Figure 6

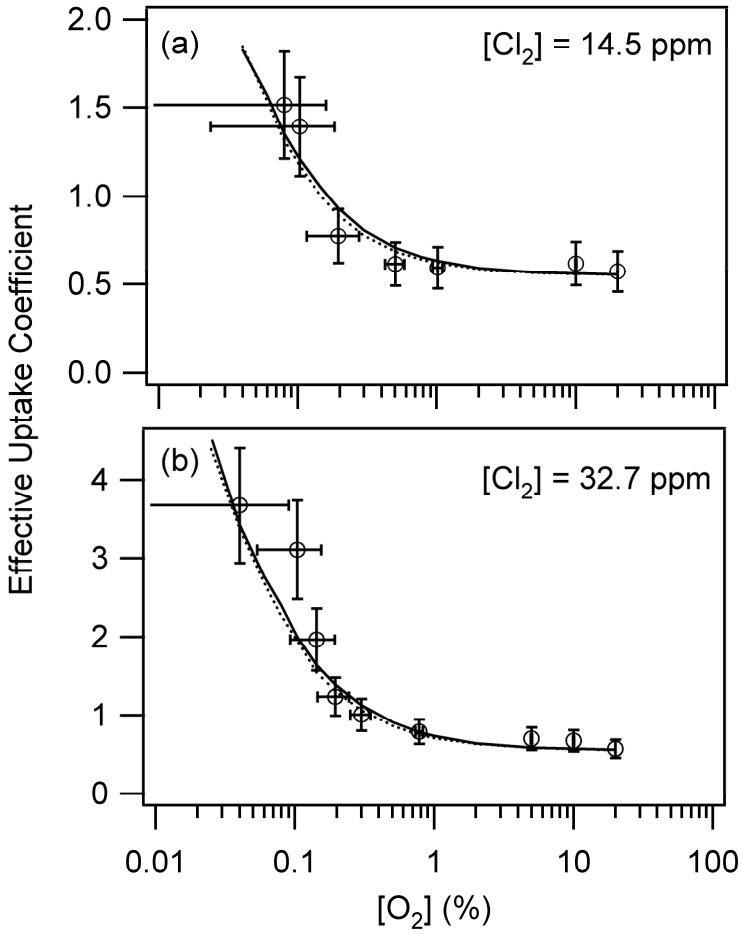
(a)
[Cl2] = 14.5 ppm
(b)
[Cl2] = 32.7 ppm
Effective Uptake Coefficient
[O2] (%)
2.0
1.5
1.0
0.5
0.0
4
3
2
1
0
0.01
0.1
1
10
100

Figure 7

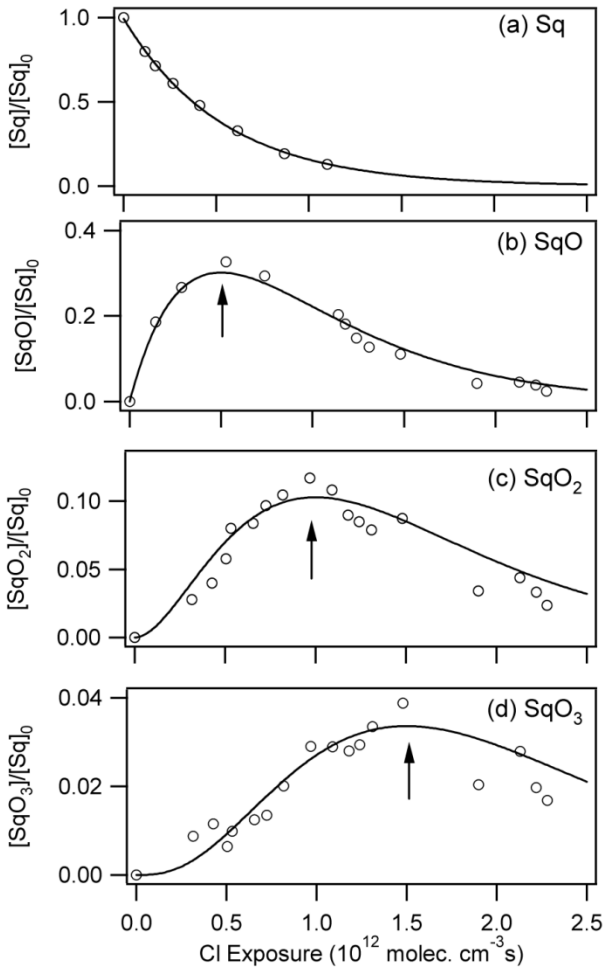
(a) Sq
(b) SqO
(c) SqO2
(d) SqO3
[Sq]/[Sq]0
[SqO]/[Sq]0
[SqO2]/[Sq]0
[SqO3]/[Sq]0
1.0
0.5
0.0
0.4
0.2
0.0
0.10
0.05
0.00
0.04
0.02
0.00
0.0
0.5
1.0
1.5
2.0
2.5
Cl Exposure (10^12 molec. cm^-3 s)

Figure 8

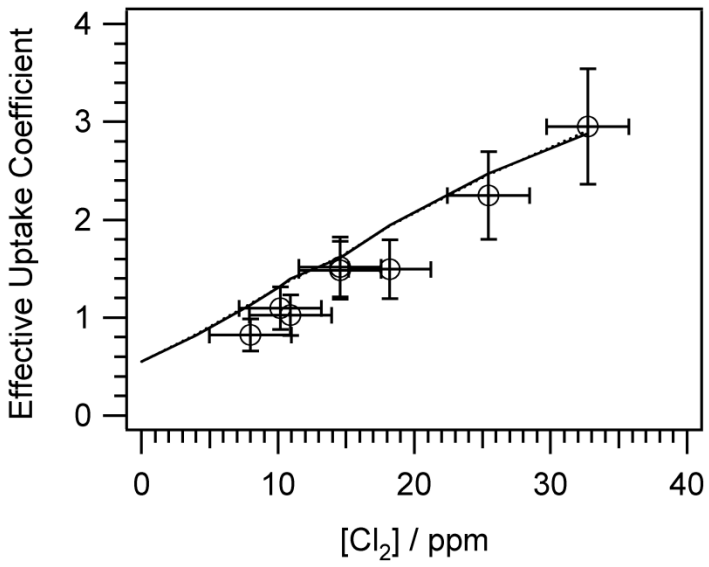

Figure 9

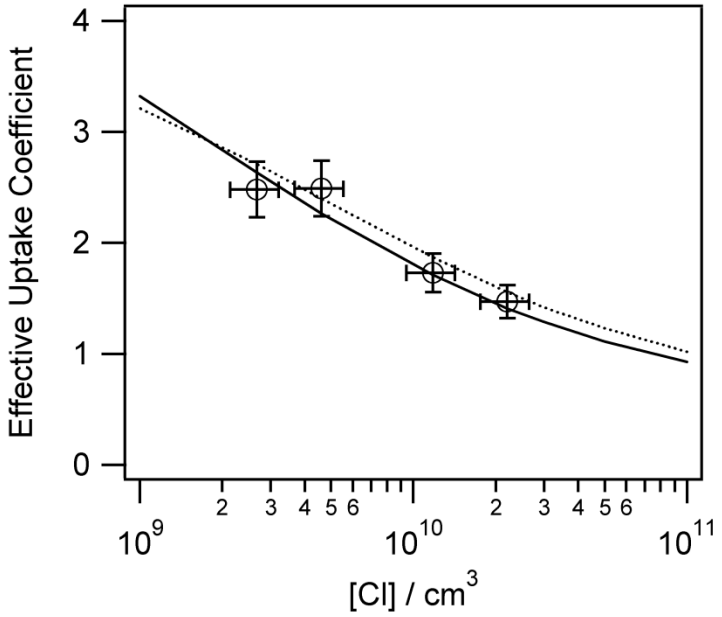
Effective Uptake Coefficient
0
1
2
3
4
10^9
10^{10}
10^{11}
2 3 4 5 6
2 3 4 5 6
[Cl] / cm^3

Figure 10

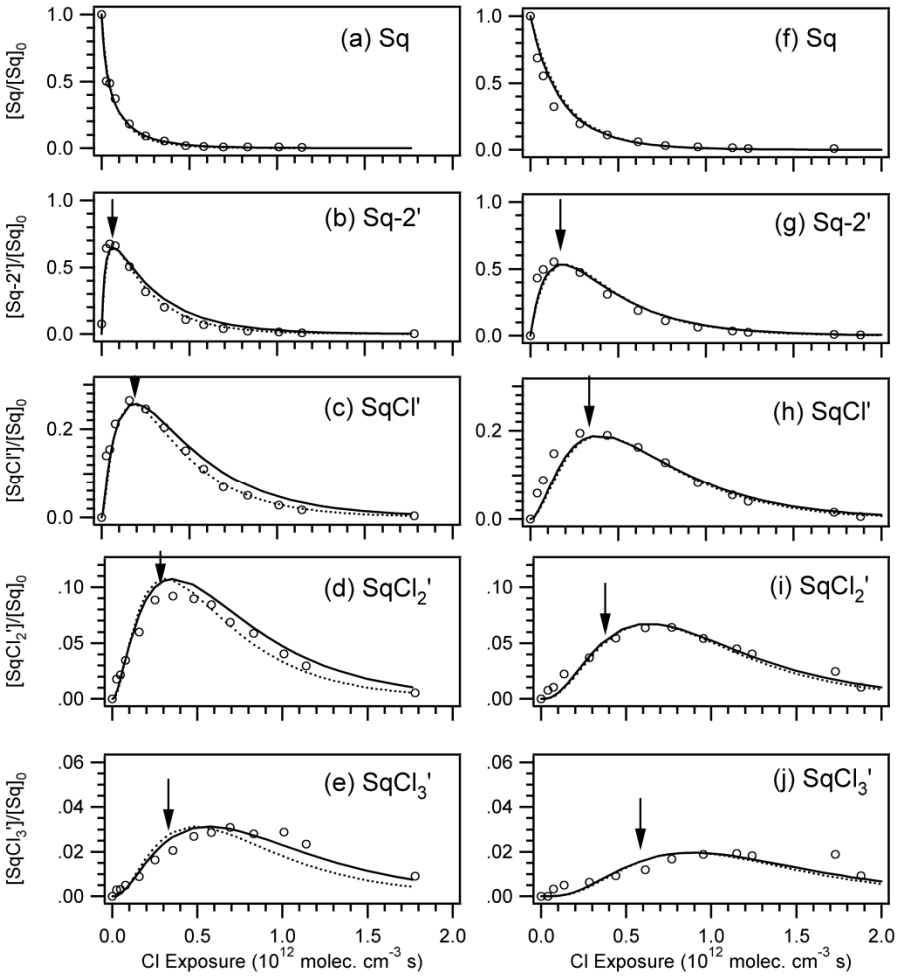
(a) Sq
(f) Sq
(b) Sq-2'
(g) Sq-2'
(c) SqCl'
(h) SqCl'
(d) SqCl2'
(i) SqCl2'
(e) SqCl3'
(j) SqCl3'
[Sq/[Sq]0
[Sq-2']/[Sq]0
[SqCl']/[Sq]0
[SqCl2']/[Sq]0
[SqCl3']/[Sq]0
Cl Exposure (10^12 molec. cm^-3 s)
Cl Exposure (10^12 molec. cm^-3 s)

Figure 11